ARTICLES

Femtosecond studies of the phase transition in Ti_2O_3

H. J. Zeiger
Department of Physics, Massachusetts Institute of Technology, Cambridge, Massachusetts 02139

T. K. Cheng and E. P. Ippen
Department of Electrical Engineering and Computer Science, Massachusetts Institute of Technology, Cambridge, Massachusetts 02139

J. Vidal
Department of Physics, Massachusetts Institute of Technology, Cambridge, Massachusetts 02139

G. Dresselhaus
Francis Bitter National Magnet Laboratory, Massachusetts Institute of Technology, Cambridge, Massachusetts 02139

M. S. Dresselhaus
Department of Electrical Engineering and Computer Science and Department of Physics, Massachusetts Institute of Technology, Cambridge, Massachusetts 02139

(Received 2 October 1995; revised manuscript received 12 January 1996)

We report femtosecond time-resolved pump-probe DECP experiments using a colliding pulse mode-locked laser performed on Ti_2O_3 as the sample lattice temperature T_L is raised from 300 K through the ''soft transition'' at 450 K to a temperature of 570 K. We have observed DECP spectra through the transition, with oscillations in reflectivity of a few percent associated with the low frequency A_{1g} mode. A thermodynamic relation is found between the low frequency A_{1g} equilibrium displacement and the number of excited electrons removed from the valence band. When applied to T_L-dependent equilibrium coordinate data for Ti_2O_3 obtained in x-ray experiments, the theory allows a determination of the band overlap vs lattice temperature. The band overlap at $T_L=621$ K is found to be ~ 0.06 eV. The A_{1g} mode frequency ν_{ph}, the electronic relaxation rate $(1/\tau_{el})$, and the phonon relaxation rate $(1/\tau_{ph})$ have all been followed through the transition. ν_{ph} decreases, and shows a partial recovery in agreement with other Raman studies. The behavior of $(1/\tau_{el})$ can be understood as due to an increase in available states for interband electron-phonon scattering as the band crossing takes place. Applying a deformation potential model to the data for $(1/\tau_{el})$ before band crossing, with the low frequency A_{1g} mode as the dominant scattering mechanism, a value of $|D|\cong 2.0$ eV is obtained for the valence band deformation potential associated with this mode. $(1/\tau_{ph})$ does not show a clearcut correlation with bandcrossing due to greater scatter in the data. The temperature dependence is partially explained by the two-phonon decay of the coherent phonon excited in DECP, and may also have a component due to interaction with hot electrons as well as a dephasing contribution. [S0163-1829(96)01625-6]

I. INTRODUCTION

We have performed temperature dependent optical pump-probe experiments on the reflectivity of the oxide compound Ti_2O_3. In earlier publications,[1,2] we reported the observation of large amplitude oscillations in the reflectivity vs time from Ti_2O_3 at room temperature, in addition to the usual exponentially decaying background due to the disturbance of the electron distribution. An oscillatory component has been observed in a number of other materials.[1,3–9] Other mechanisms can produce such structure, but strong A_1 oscillations are due to what we have termed displacive excitation of coherent phonons (DECP).[1,2] In this paper, we report changes in DECP as the temperature is increased through the ''soft'' phase transition of Ti_2O_3 at ~ 450 K.

Since the discovery[10] that Ti_2O_3 undergoes a soft phase transition with no change of symmetry, a large body of experimental work on this transition has been reported in the literature. This includes studies of changes in lattice parameters,[11] specific heat,[12] Raman scattering,[13] optical properties,[14] and transport properties.[15–17] It is now generally accepted that the transition is due to the crossing of bands at different points in the Brillouin zone as the temperature is increased,[18] with the resulting disappearance of an energy gap. Theoretical calculations have indicated that there should be no energy gap according to conventional band calculations,[19] and that electron-electron correlation energy must be included to explain the presence of a gap below ~ 450 K. The true nature of the phase transition is still not well understood, although attempts to model it have been made involving lattice energy, and electron-electron correlation energy.[20,21]

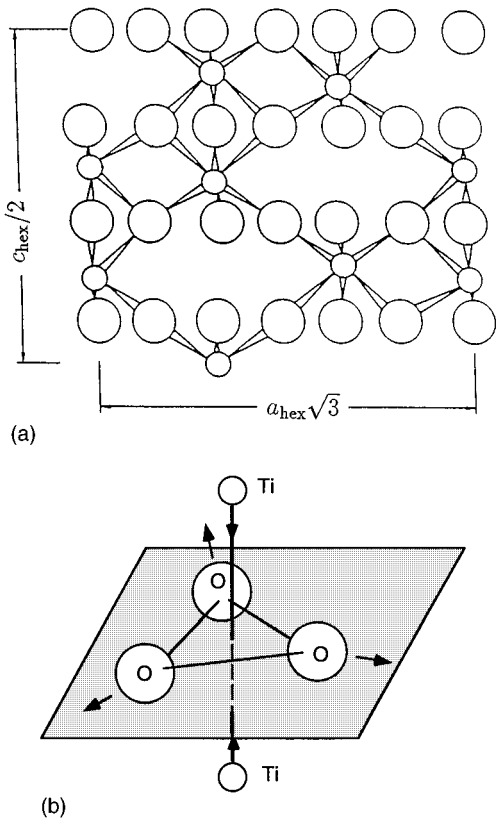

FIG. 1. (a) The corundum structure. The large and small circles, respectively, represent oxygen and titanium atoms. Note that the positions of the Ti atoms are not entirely determined by the structure itself. (b) A schematic picture of the motion of Ti and O atoms in the low frequency A_{1g} vibration.

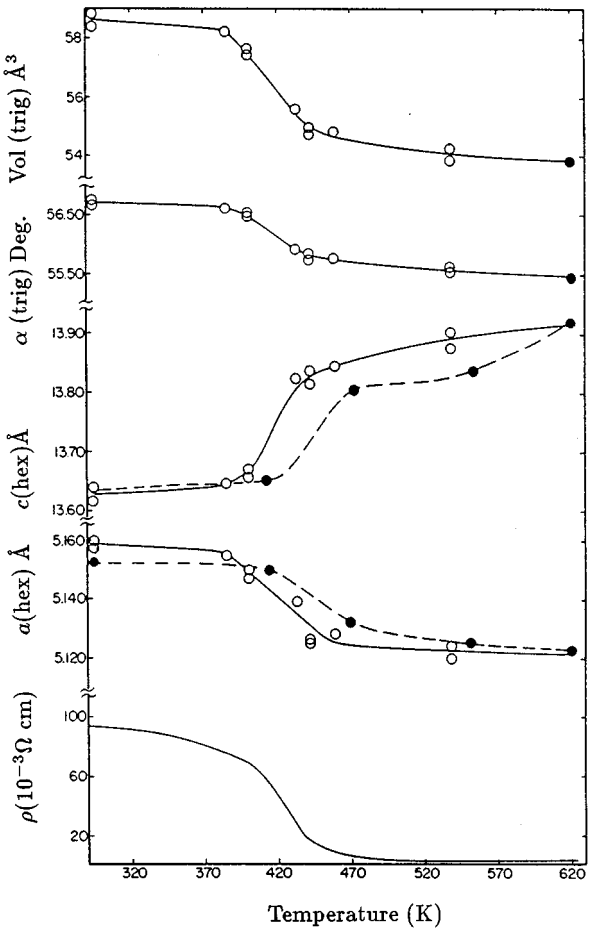

FIG. 2. Plots of lattice parameters and resistivity vs temperature observed in Ti_2O_3 (after Ref. 10).

Figures 1(a) and 1(b), respectively, show the corundum structure of Ti_2O_3 and the nature of the low frequency A_{1g} mode. Figure 2 presents the behavior of lattice parameters and resistivity through the soft transition. Although the properties of Ti_2O_3 have been extensively studied experimentally, many details of the band structure have not been well established quantitatively. The energy gap at 300 K has been reasonably well determined at ~ 0.15 eV,[14,22] with the gap going to zero at ~ 450 K. X-ray studies have given accurate determinations of the *a*- and *c*-lattice parameters of the material through the transition, as well as changes in titanium and oxygen positions.[11] However, many different estimates of the hole and electron masses have been given,[15,22] some of them contradictory, and there is even uncertainty in the hole and electron number densities as a function of temperature.[22]

In this paper we present a study of DECP in Ti_2O_3 as the temperature of the sample is increased from 300 K through the soft phase transition and up to 567 K. From a fit of the data at each temperature to an empirical description of the DECP process developed in Ref. 2 we obtain values of the parameters of the model. In particular, we obtain values of $1/\tau_{el} \equiv \beta$ and $1/\tau_{ph} \equiv \gamma$ (respectively, effective electron and phonon relaxation rates) as a function of the sample temperature (see Sec. II).

It is found that $1/\tau_{el}$ follows qualitatively a temperature dependence similar to the sample conductivity, increasing by about a factor of 3 as the sample temperature is raised through the soft transition. Although other explanations and interpretations of this behavior may be possible, we find that it can be understood in terms of the energy relaxation rate of excited carriers, which increases because of increasing interband components due to an increase of available states for scattering as the bands cross.

$1/\tau_{ph}$ shows no clear correlation with the resistivity as the temperature is raised through the transition. However, there is considerable scatter in the data points. The temperature dependence can be understood as due to a combination of two-phonon decay of the A_{1g} coherent phonon, along with a possible hot electron decay process, as well as dephasing.

We also study a thermodynamic model of Ti_2O_3 which relates the equilibrium value of the low frequency A_{1g} coordinate q to the number of electrons in excited bands. The model is based on a balance between the increase in core free energy due to an increase in q and a decrease in deformation potential free energy of conduction electrons when carriers are transferred between bands. It is shown that the model can be interpreted as also including a contribution due to carrier charge redistribution if the model parameters are interpreted as effective parameters. When applied to equilibrium x-ray measurements of ion coordinates as a function of lattice temperature, the model yields a measurement of conduction and valence band overlap as a function of temperature. The re-

sults are also applied to a description of the DECP process.

In Sec. II of this paper, we summarize the DECP model results obtained in Ref. 2. The experimental results are given in Sec. III. Section IV presents the derivation of the thermodynamic relationship. Sections V and VI, respectively, discuss theoretical descriptions of the electron and phonon relaxation rates, and in Sec. VII we consider further implication of the DECP process.

II. THEORY OF DECP

We will summarize briefly the results obtained in Refs. 1 and 2 for the theory of DECP that are relevant to the study of Ti_2O_3 described in this paper. The idea is that when a pump pulse of short duration ($\sim$60 fs) arrives at the surface of a conductor or semiconductor, the electronic system is disturbed, but comes to equilibrium in a time short compared to the response time of the nuclei. Now, if the lattice allows displacements of A_1 or A_{1g} symmetry, then such displacements preserve the symmetry of the unit cell. At equilibrium before the arrival of the pump pulse, the A_1 nuclear displacements within the unit cell are determined by the minimization of free energy. When the system is suddenly excited by the pump pulse, new equilibrium A_1 nuclear displacements result. The nuclear system, attempting to return to equilibrium, is therefore set into coherent A_1 oscillation about the new equilibrium A_1 positions. If the lattice has more than one A_1 mode of oscillation, then each mode will be driven to the extent that it is represented in the new equilibrium displacement of the lattice. Except in very unusual circumstances, or with very intense pump pulses, modes of symmetry other than A_1 or A_{1g} will not be excited, since their excitation would require equilibrium displacements which would change the lattice symmetry.

The electronic excitation which causes the change in the equilibrium A_1 coordinates can be described in terms of the number of electrons per unit volume, $n(t)$, which are left in an excited band, or the change in electron temperature, $\Delta T_{\rm el}(t)$, or some other measure of electronic excitation. The electronic excitations decay exponentially with time. With the hypothesis that the change in A_1 equilibrium displacement is proportional to some measure $n^\star(t)$ of electronic excitation, the classical equations of motion of the A_1 modes can be solved. Both the direct effect of the electronic excitation and the secondary effect due to the coherent A_1 mode oscillation produced by the electronic excitation lead to a modulation of the dielectric response of the medium, and hence oscillations in the reflectivity are observed.

The measured reflectivity signal as a function of time is the true reflectivity change convolved with the pump-probe autocorrelation function. The result obtained for the fractional change in reflectivity measured from the arrival of the peak of the pump pulse is[2]

$$\frac{\overline{\Delta R(t)}}{R}=A\int_0^\infty G(t-\tau)e^{-\beta\tau}d\tau+\frac{B\omega_0^2}{\omega_0^2+\beta^2-2\gamma\beta}\int_0^\infty G(t-\tau)\left\{e^{-\beta\tau}-e^{-\gamma\tau}\sqrt{1+\left(\frac{\beta'}{\Omega}\right)^2}\cos(\Omega\tau+\Phi)\right\}d\tau+C\int_0^\infty G(t-\tau)d\tau. \tag{1}$$

$G(t)$ is the pump-probe autocorrelation function. The first term on the right-hand side represents the direct effect of the electronic excitation, and the second term the indirect effect due to the A_1 equilibrium displacement produced by the electronic excitation. The third term contains a parameter C meant to represent the effect of the sample heating or the trapping of electrons in an excited band, both of which can shift the baseline of the spectrum. γ is an effective decay constant for the coherent A_1 phonon of angular frequency ω_0 that is excited. β represents a decay constant for the electronic excitation, and the angular frequency Ω and the effective decay constant β' are defined as

$$\Omega=\sqrt{\omega_0^2-\gamma^2} \tag{2}$$

and

$$\beta'=\beta-\gamma. \tag{3}$$

The phase shift Φ is given by the relation $\tan\Phi=\beta'/\Omega$.

The coefficients A and B in Eq. (1) can be written as

$$A=\frac{1}{R}\left(\frac{\partial R}{\partial n^*}\right)\rho\varepsilon_{\rm pump}, \tag{4}$$

$$B=\frac{1}{R}\left(\frac{\partial R}{\partial q}\right)\kappa\rho\varepsilon_{\rm pump}, \tag{5}$$

where the reflectivity R is a function of the complex dielectric constant $\varepsilon=\varepsilon_1+i\varepsilon_2$. Here $n^\star$ denotes some measure of electronic excitation; and q is the A_{1g} coordinate. In Eqs. (4) and (5), $\varepsilon_{\rm pump}$ is the integrated energy per unit area in the pump pulse, ρ is a measure of the excitation produced at the surface due to the pump, and κ is the proportionality constant $\Delta q/n^\star$ produced by the electronic excitation. If there is more than one A_1 mode, there is a different κ for each mode excited by the electronic disturbance. The values of the parameters A and B for Ti_2O_3, at room temperature are $A=2.6\times10^{-2}$, $B=-5.7\times10^{-2}$.

We will see in Sec. III that the experimental data over the entire temperature range through the soft transition in Ti_2O_3 are well represented by Eq. (1) (except perhaps for long time delays, see Sec. IV) with decay constants β and γ which vary with the Ti_2O_3 temperature T_L before the arrival of the pump pulse. Furthermore, the change in β with changing T_L through the transition is strongly correlated with the collapsing energy gap ϵ_g. An excellent fit of the observed spectra in Ti_2O_3 for times up to a few picoseconds and at all temperatures was obtained using Eq. (1).

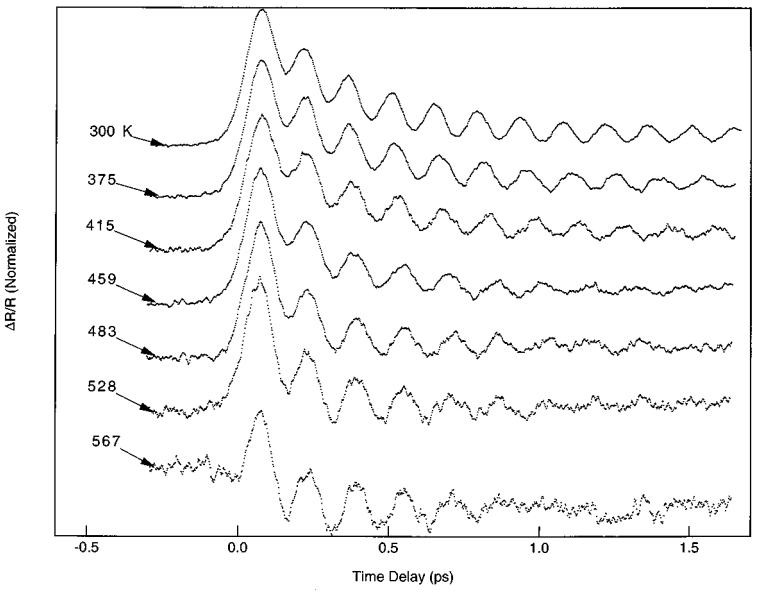

FIG. 3. Plots of $\overline{\Delta R}/R$ vs time measured in a DECP experiment in Ti_2O_3 at temperatures ranging from 300 K to 570 K.

III. EXPERIMENTAL STUDIES OF DECP

All experiments were carried out with a dispersion-compensated colliding pulse mode-locked laser source[23] (CPM) in a standard two-pulse pump-probe configuration.[24] The CPM laser generates transform-limited pulses which are 60 fs in duration, 2 eV in photon energy, total energy per pulse of 10 pJ, and 80 MHz in repetition rate. In the pump-probe experiment, the CPM output is split into pump pulses, which optically excite the sample, and weaker variably delayed probe pulses, which measure the pump-induced changes in the optical properties of the sample. All of the data shown in this paper monitor the transient reflectivity behavior of single-crystal Ti_2O_3 oriented with the c axis parallel to the direction of light propagation. Temperature dependent pump-probe data were obtained by mounting the Ti_2O_3 crystal on a feedback-controlled resistive heating element. A thermocouple was used to monitor the temperature of the copper block on which the sample was mounted over the temperature range 300–570 K with an estimated error of ± 20 K.

Figure 3 shows the temperature dependent pump-probe reflectivity data for Ti_2O_3. In each case, we find that the pump initially causes a sharp decrease in the sample reflectivity followed by a sub-picosecond time scale recovery. Superimposed on this recovery is a strong oscillatory feature which corresponds to the pump-induced coherent phonon modulating the index of refraction. We note that we only observe coherent phonons of A_{1g} symmetry as is expected from the DECP model.

The pump-probe data have been least-squares fitted to the DECP model [Eq. (1)] at each temperature to give the parameters $1/\tau_{\rm el} \equiv \beta$, $1/\tau_{\rm ph} \equiv \gamma$, and $\nu_{\rm ph} = \omega_0/2\pi$. Because the coherent phonon oscillations occur at a frequency not much greater than the excitation pulse bandwidth, all fits had to be obtained by convolving the autocorrelation function of the pump pulse with the DECP impulse response. Without the convolution fit, the magnitude of the coherent phonon amplitude would be severely underestimated due to the finite bandwidth of the pump and probe.

The most striking features of the data are the temperature dependent behavior of the coherent phonon frequencies ($\nu_{\rm ph}$), the effective coherent phonon relaxation rate ($1/\tau_{\rm ph}$), and the effective electron relaxation rate ($1/\tau_{\rm el}$) shown respectively in Figs. 4, 5, and 6. The coherent phonon frequencies agree excellently with phonon frequencies at the lattice temperature T_L measured by conventional Raman scattering. The frequency of the coherent A_{1g} mode decreases with increasing T_L by $\sim 10\%$ through the semiconductor-metal transition and at higher temperatures the A_{1g} frequency increases again. The effective electron relaxation rate increases from $\sim 3\times 10^{12}$ s^{-1} to $\sim 10\times 10^{12}$ s^{-1} as the material turns semimetallic. To demonstrate the correlation of $(1/\tau_{\rm el})$ with the collapse of the energy gap, the inset in Fig. 6 shows a plot of ϵ_g vs T_L deduced from x-ray data (see Sec. IV).

IV. THERMODYNAMIC RELATIONSHIPS

In this section we discuss the origin of the shift in equilibrium value of q for the low frequency A_{1g} mode in Ti_2O_3 (hereafter referred to as the A_{1g} mode) as a function of lattice temperature and electronic excitation. In general, two possible sources of this shift seem to be likely candidates. The first is the redistribution of charge in $\vec{k}$ space due to excitation of carriers, leading to a corresponding spatial redistribution of charge in the crystal, and a shift in the equilibrium value of q. This charge redistribution effect should, in first approximation, be proportional to the number of excited carriers, but also should be affected by their distribution in excited bands. A preliminary calculation of the effect of charge distribution on A_{1g} equilibrium displacement for the case of Sb was performed in collaboration with Gonze's group at the University of Louvain.[25] This work was based on first principles pseudopotential calculations of Gonze *et al.*[26]

The second mechanism for a shift in equilibrium value of q which we consider is based on the thermodynamic balance between the free energy rise due to core electrons when q is increased from its equilibrium value, and the deformation potential decrease of the free energy when valence electrons are transferred to an excited band.

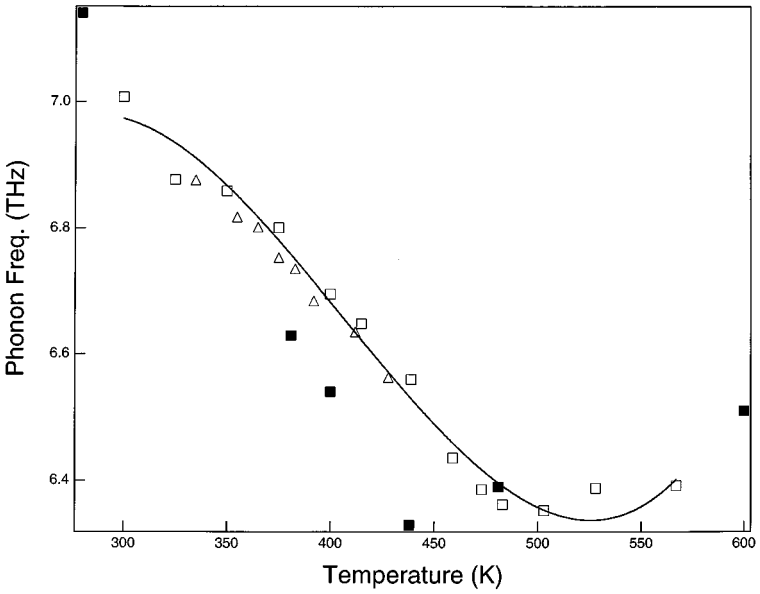

FIG. 4. Plot of the A_{1g} mode frequency vs temperature measured in a DECP experiment in Ti_2O_3. Open squares and triangles represent two DECP runs. Black squares show Raman scattering results (after Ref. 13).

We find that the application of these two mechanisms to a description of the change in equilibrium Ti-Ti pair distance as a function of temperature T_L as measured in x-ray diffraction experiments allows a determination of ϵ_g vs T_L through the band crossing. We also find that the model allows a measurement of the change in q produced in pump-probe experiments, and provides a description of the DECP experiments.

The model of Ti_2O_3 that we use is based on the band crossing model of Goodenough,[18] and the band structure calculations of Ashkenazi and Weger.[19] A schematic picture of the relevant bands is shown in Fig. 7. At room temperature, the valence band (2) is partly filled, and the conduction band (1), which is separated from band (2) by an indirect gap ϵ_g of about 0.15 eV, is partly empty. According to the calculation of Ref. 19, bands (1) and (2) would overlap if it were not for the electron-electron interaction. We assume that the value of gap at a given temperature T_L depends on all thermodynamic variables, including the normal mode coordinates of the material. Thus, we will argue that the static, equilibrium value of ϵ_g at a given temperature, is determined by the minimization of the free energy with respect to all thermodynamic variables including coordinates $q^{(\alpha)}$, where α labels the different modes. But, as the A_{1g} coordinate q alone varies during DECP, the energy gap is modulated according to an optical mode deformation potential associated with this A_{1g} mode. The motion of the titanium and oxygen atoms in the A_{1g} mode is shown in Fig. 1(b). We take the distance between the Ti atoms in this mode displacement as a measure of q.

According to the band structure calculations there is no single transition dominating the dielectric behavior of Ti_2O_3 at 2 eV. Furthermore, both real and imaginary parts of the dielectric constant[27] of Ti_2O_3 at 2 eV are small, and show maxima at ~ 1 eV and ~ 4 eV. We therefore expect

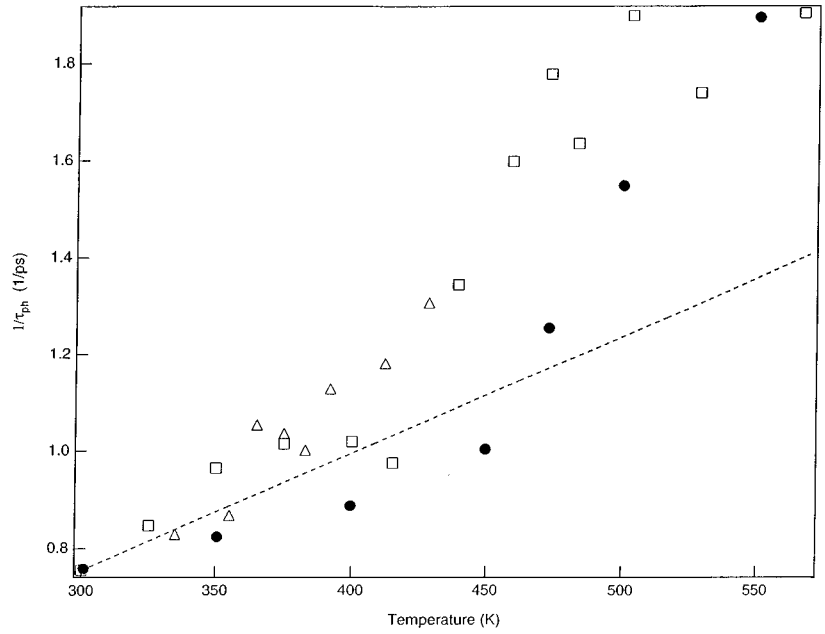

FIG. 5. Plot of $1/\tau_{ph}$ vs temperature measured in a DECP experiment in Ti_2O_3. The dashed line shows the result calculated for two-phonon decay alone. Black circles represent the fit to Eq. (77) (see text, Sec. VI).

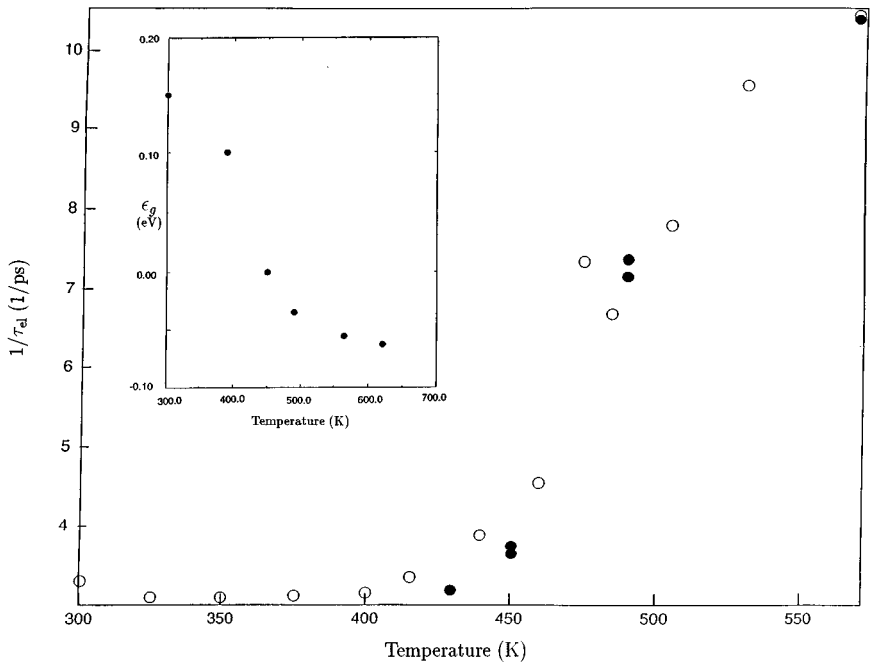

FIG. 6. Plot of $1/\tau_{\rm el}$ vs temperature measured in DECP experiments in Ti_2O_3. Open circles are the data. The black circles are the results of calculations based on Eq. (56). The black circle at $T_L \sim 430$ K is the point at which the contribution due to interband scattering vanishes (see text, Sec. V). The inset shows ϵ_g vs T_L determined from x-ray data, using the parameter value $(N_1/N_2)(m_1^\star/m_2^\star)^{3/2}=2$ (see text, Sec. IV).

that only a fraction of the excited carriers come from the vicinity of the valence band (2); and, indeed, the pump-probe spectrum observed in Ti_2O_3 at room temperature shows a fast component up to about a few ps after the pump pulse, and much later a relatively small slow component. The change in relaxation rate of the initial, fast component roughly follows the temperature dependence of the energy gap in Ti_2O_3 indicated by other experiments,[14] so we assume that this portion of the spectrum relates to the relaxation of the carriers associated with the fraction of the excited carriers in bands (1) and (2). In the following discussion we take the Ti_2O_3 samples to be nearly intrinsic, so that, at least at thermal equilibrium, the number of holes in band (2) equals the number of electrons in band (1).

We denote the lattice coordinate of the $A_{1g\not}$ mode as q (essentially characterized by the Ti-Ti pair separation associated with the $A_{1g\not}$ mode); and all other modes, both optical and acoustic, by the designation $q^{(\alpha)}$. It will be convenient to consider first the effect of the thermodynamic balance on the shift in equilibrium value of q. During the DECP process, all the acoustic modes of the system will be constrained, and only the displacement q of the $A_{1g\not}$ mode will be important. We therefore write the free energy per unit volume of the system at temperature T_L due to the displacement q, and excluding the contribution of the carriers in bands (1) and (2), as

$$F_L(q)=n_0 a_L(q-q_{\rm eq}^0)^2-n_0 b_L(q-q_{\rm eq}^o)^3+\cdots. \qquad (6)$$

Here, $q_{\rm eq}^0$ is the equilibrium value of the $A_{1g\not}$ coordinate at the temperature T_L from F_L alone; n_0 is the number of Ti_2O_3 molecules per unit volume; and a_L represents a force constant for the $A_{1g\not}$ mode. The term proportional to b_L is due to anharmonicity. We assume for simplicity that a_L, b_L, and $q_{\rm eq}^0$ have only a weak dependence on T_L.

We must now consider the dependence on the $A_{1g\not}$ coordinate of the free energy per unit volume due to carriers in bands (1) and (2). These bands are not well characterized, either theoretically or experimentally. A variety of masses ranging from $(m^*/m)\sim 2$ to 5 and larger have been reported in the literature.[15,22] $A_{1g\not}$ deformation potentials for the bands are not known, but we will assume that bands (1) and

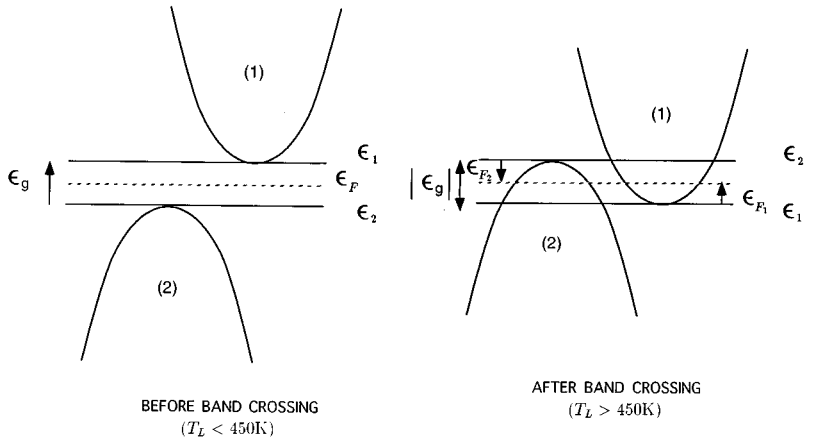

FIG. 7. A schematic picture of the relevant conduction and valence bands of Ti_2O_3 before and after band crossing.

(2) can be characterized by deformation potentials D_1 and D_2, respectively. The signs and magnitudes of D_1 and D_2 are not known, but we will shortly see that it is reasonable to assume that a deformation potential $2D=D_1-D_2$, which describes the modulation of ϵ_g, is negative. This means that an increase in q produces a decrease in ϵ_g. The deformation potentials will be taken as nearly constant through the entire lattice temperature range from 300 K, where Ti_2O_3 has an indirect band gap of $\sim$0.15 eV, to $\sim$600 K, where the bands have crossed. The $A_{1g\ell}$ optical mode deformation potentials D, in analogy with the usual definition of acoustic mode deformation potentials, will be defined by the relation

$$\Delta\epsilon = D\frac{\Delta q}{q_0}, \tag{7}$$

where $\Delta\epsilon$ is the change in energy of the band edge, Δq is the change in Ti-Ti pair separation associated with $A_{1g\ell}$, and q_0 is taken for convenience as the pair separation at room temperature, $\sim$2.6 Å.

The free energy of the carriers in bands (1) and (2) will be described by a statistical distribution characterized by a temperature T_L before the arrival of a pump pulse. Although there is experimental evidence[28] that excited electrons in pump-probe experiments cannot always be described in terms of an electron temperature, we make the simplifying assumption that after the arrival of the pump pulse the carriers are characterized by an effective temperature $T_{\rm el}$. The electron free energy expression we will use is therefore based on the usual thermodynamic relation

$$\mathcal{F} = -(k_BT)\sum_i \ln[1+e^{-\beta(\epsilon_i-\epsilon_F)}]+N\epsilon_F, \tag{8}$$

where N is the number of electrons, $\beta=1/k_BT$, ϵ_F is the Fermi energy, and ϵ_i is the energy of the ith electron state. Applying this expression to bands (1) and (2), the electronic free energy per unit volume at any temperature can then be written (see Fig. 7)

$$\begin{aligned} F_{\rm el} = &-(k_BT)N_1\int_0^\infty \rho_1(\epsilon)\ln[1+e^{-\beta(\epsilon+\epsilon_1-\epsilon_F)}]d\epsilon \\ &-(k_BT)N_2\int_0^\infty \rho_2(\epsilon)\ln[1+e^{-\beta(\epsilon-\epsilon_2+\epsilon_F)}]d\epsilon \\ &-N_2\int_0^\infty \rho_2(\epsilon)[\epsilon-\epsilon_2]d\epsilon. \end{aligned} \tag{9}$$

In Eq. (9), the first term on the right is the free energy of electrons in band (1), and the second term is the free energy of the holes in band (2). N_1 and N_2 are, respectively, the number of conduction and valence bands. Both bands are characterized by density of states factors $\rho(\epsilon)$, but in the first integral ϵ is measured up from the bottom of the band, while in the second and third integrals ϵ is measured down from the top of the band. ϵ_1 and ϵ_2 are respectively the energies of the conduction and valence band edges. ϵ_g is taken positive when the bands are not crossed. The third term on the right in Eq. (9) is the contribution of the filled band (2) to the electronic free energy of the system, introduced when the free energy of holes in band (2) was separated off. Since this term does not vary with temperature, we can assume that it has been included in the elastic free energy, Eq. (6). It contributes a temperature independent shift to $q_{\rm eq}^0$. Equation (9) does not include correlation energy, which is believed to be responsible for the presence of an energy gap below 450 K.[19]

In addition to the q dependence of the electronic free energy of the system, the q dependence of the phonon free energy should be included in considering the equilibrium value of the q coordinate. This free energy can be written

$$F_{\rm ph} = \sum_{\ell} (k_BT)\int_0^\infty \rho_\ell(\hbar\omega)\ln[1-e^{-\beta\hbar(\omega_{0\ell}+\omega)}]d(\hbar\omega). \tag{10}$$

In Eq. (10), the sum over ℓ represents a sum over branches of the phonon spectrum, and $\omega_{0\ell}$ is the lowest frequency point in the ℓth branch. The phonon branches do show a softening of about 10–15 % through the transition, but as we shall see, this could be mainly due to the anharmonic term in the elastic free energy of Eq. (6).

The equilibrium condition for the system free energy with respect to changes in the $A_{1g\ell}$ mode coordinate q is

$$\left(\frac{dF}{dq}\right)=\left(\frac{dF_L}{dq}\right)+\left(\frac{dF_{\rm el}}{dq}\right)+\left(\frac{dF_{\rm ph}}{dq}\right)=0. \tag{11}$$

We first treat the case where the entire system is at equilibrium at temperature T_L. Using partial integration of some terms, the derivative of $F_{\rm el}$ with respect to q can be written

$$\begin{aligned} \left(\frac{dF_{\rm el}}{dq}\right) = &\int_0^\infty\left[\rho_1(\epsilon)\frac{d\epsilon_1}{dq}-\frac{dN_1(\epsilon)}{dq}\right]f_1(\epsilon)d\epsilon \\ &+\int_0^\infty\left[-\rho_2(\epsilon)\frac{d\epsilon_2}{dq}-\frac{dN_2(\epsilon)}{dq}\right]f_2(\epsilon)d\epsilon, \end{aligned} \tag{12}$$

where

$$\begin{aligned} f_1(\epsilon) &\quad [1+e^{\beta(\epsilon+\epsilon_1-\epsilon_F)}]^{-1}, \\ f_2(\epsilon) &\quad [1+e^{\beta(\epsilon-\epsilon_2-\epsilon_F)}]^{-1}. \end{aligned} \tag{13}$$

In Eq. (12), $N(\epsilon)$ is the integrated density of states up to energy ϵ. If the changes in ϵ_1 and ϵ_2 with q are given, respectively, by the deformation potentials D_1 and D_2, then Eq. (12) can be rewritten,

$$\left(\frac{dF_{\rm el}}{dq}\right)=n\left(\frac{D_1}{q_0}\right)[1+\eta_{e_1}]-n\left(\frac{D_2}{q_0}\right)[1+\eta_{h_2}]. \tag{14}$$

In Eq. (14), the additional factors η_{e_1} and η_{h_2} come from the contributions of $dN_1(\epsilon)/dq$ and $dN_2(\epsilon)/dq$ in Eq. (12), respectively. Although the contributions of $\rho_1(\epsilon)$ and $\rho_2(\epsilon)$ in Eq. (12) are proportional to n, and therefore independent of the actual distribution of carriers, the η terms in Eq. (14) are dependent on the statistical distribution of carriers as well as carrier number. Near indirect band edges, where bands move almost rigidly with q, we expect $dN(\epsilon)/dq$ to be small. Hence, the $\eta's$ should be small at equilibrium for small band overlap.

It is difficult to evaluate how large an effect the q dependence of the phonon free energy, Eq. (10), has on the equilibrium shift of q with temperature. The decrease observed in

Raman frequencies through the soft phase transition is 10–15 %, and, as we will see, this could be due to the change in n through the transition. In any case, the change seems to be at least roughly proportional to n, and so we will assume that, if not negligible, it can be lumped into Eq. (14) in the form of possible corrections to the deformation potentials D_1 and D_2. From Eq. (14), we then have the equilibrium condition,

$$2n_0a_L(q-q_{\rm eq}^0)-3n_0b_L(q-q_{\rm eq}^0)^2+n\left(\frac{D_1}{q_0}\right)[1+\eta_{e_1}] -n\left(\frac{D_2}{q_0}\right)[1+\eta_{h_2}]=0. \tag{15}$$

Neglecting first the anharmonic term in Eq. (15), the resulting shift in equilibrium value of q is

$$\Delta q_{\rm eq}\cong\frac{1}{2a_L}\left[-\left(\frac{n}{n_0}\right)\left(\frac{2\overline{D}}{q_0}\right)-\left(\frac{n_{e_1}}{n_0}\right)\left(\frac{D_1}{q_0}\right)\eta_{e_1} +\left(\frac{n_{h_2}}{n_0}\right)\left(\frac{D_2}{q_0}\right)\eta_{h_2}\right], \tag{16}$$

where $n=n_{e_1}=n_{h_2}$, and $2\overline{D}\equiv D_1-D_2$.

a_L can be eliminated from Eq. (16) if we write the equation of motion for the A_{1g} mode in terms of the reduced mass μ,

$$\mu n_0\ddot{q}=-\frac{\partial F}{\partial q}\simeq-2a_Ln_0(q-q_{\rm eq}^0). \tag{17}$$

The angular frequency ω_0 of the A_{1g} mode is then given by the relation

$$\omega_0^2\mu\cong 2a_L. \tag{18}$$

Substitution in Eq. (16) yields

$$\Delta q_{\rm eq}\cong\frac{1}{\omega_0^2\mu}\left[-\left(\frac{n}{n_0}\right)\left(\frac{2\overline{D}}{q_0}\right)-\left(\frac{n_{e_1}}{n_0}\right)\left(\frac{D_1}{q_0}\right)\eta_{e_1} +\left(\frac{n_{h_2}}{n_0}\right)\left(\frac{D_2}{q_0}\right)\eta_{h_2}\right]. \tag{19}$$

We can now rewrite the total free energy, $F=F_L+F_{\rm el}$, in terms of the new equilibrium position

$$q'_{\rm eq}\equiv q_{\rm eq}^0+\Delta q_{\rm eq}$$

by replacing $(q-q_{\rm eq}^0)$ in the free energy by $(q-q'_{\rm eq}+\Delta q_{\rm eq})$ and expanding in powers of $\Delta q_{\rm eq}$, keeping terms up to second order in $(q-q'_{\rm eq})$. We find

$$F=n_0a_L\left[1-\frac{3b_L}{a_L}\{\Delta q_{\rm eq}^n+\Delta q_{\rm eq}^{n'}\}\right](q-q'_{\rm eq})^2, \tag{20}$$

where

$$\Delta q_{\rm eq}^n=-\frac{1}{\omega_0^2\mu}\left(\frac{2\overline{D}}{q_0}\right)\left(\frac{n}{n_0}\right), \tag{21}$$

$$\Delta q_{\rm eq}^{n'}=\frac{1}{\omega_0^2\mu}\left[-\left(\frac{D_1}{q_0}\right)\left(\frac{n_{e_1}}{n_0}\right)\eta_{e_1}+\left(\frac{D_2}{q_0}\right)\left(\frac{n_{h_2}}{n_0}\right)\eta_{h_2}\right]. \tag{22}$$

Equation (21) is a term proportional to the number of electrons transferred from band (2) to band (1), and Eq. (22) represents a correction due to the distribution of carriers in these bands. These two terms produce a shift in Raman frequency through the presence of anharmonicity, as well as a shift in equilibrium value of q.

We now consider the effect of charge redistribution on the shift in equilibrium value of the A_{1g} coordinate q. As noted earlier, in the first approximation we expect the shift to be proportional to the number of carriers transferred, but also to depend somewhat on how the carriers are distributed in the bands. But these effects can be included by interpreting the parameters D_1, D_2, and η_{e_1}, η_{h_2} in $\Delta q_{\rm eq}$ given in Eq. (16) as *effective* parameters. In that case, Eqs. (19)–(22) can be interpreted as describing the effect of both charge redistribution and thermodynamic balance.

Equation (20) could explain the decrease in Raman frequency of $\sim$10% observed in all modes of Ti_2O_3 in the vicinity of 450 K. As the temperature is raised through the soft transition, $\Delta q_{\rm eq}^n$ and $\Delta q_{\rm eq}^{n'}$ increase in magnitude in proportion to the change in number of carriers at equilibrium. Consequently, through anharmonicity all the Raman modes show a decrease in frequency near the transition which approximately mirrors the change in carrier concentration.

During the course of the A_{1g} vibration, the energy gap will be modulated according to the deformation potential $2\overline{D}$. Before band crossing, the electron distribution between bands (1) and (2) is not likely to adjust to the time-varying equilibrium requirements, since the relaxation time for equilibration between bands (1) and (2) should be long compared to a vibration period. However, at a temperature T_L greater than 450 K, when the bands have crossed, it is possible that the interband relaxation time τ_I could become comparable to or shorter than a vibration period. This would imply a spatial redistribution of charge, corresponding to the charge redistribution in $\vec{k}$ space, at terahertz frequencies. In DECP, the large amplitude oscillating charge produced could generate radiation in a material with an A_1 mode, which does not have a center of inversion symmetry.

The attempt of the population of band carriers to follow the modulation of the energy gap can produce both an A_{1g} frequency shift and a contribution to A_{1g} damping. This problem has been considered by Cerdeira and Cardona.[29] If τ_I (referred to as τ_R by Cerdeira and Cardona) is the carrier number relaxation time for interband transitions, then the result is a correction to the frequency given by

$$\frac{\Delta\omega}{\omega_0}\cong\frac{1}{2}\frac{1}{[1+(\omega_0\tau_I)^2]}\left(\frac{1}{n_0\omega_0^2\mu}\right)\left(\frac{2\overline{D}}{q_0}\right)^2\left(\frac{dn}{d\epsilon_g}\right)_{q'_{\rm eq}} \tag{23}$$

and a contribution to the A_{1g} phonon damping in the form of a relaxation rate

$$\frac{1}{\omega_0\tau_{\rm ph}}=-\frac{1}{2}\frac{\omega_0\tau_I}{[1+(\omega_0\tau_I)^2]}\left(\frac{1}{n_0\omega_0^2\mu}\right)\left(\frac{2\overline{D}}{q_0}\right)^2\left(\frac{dn}{d\epsilon_g}\right)_{q'_{\rm eq}}. \tag{24}$$

In Eqs. (23) and (24) we have introduced

$$\left(\frac{dn}{dq}\right)_{q'_{eq}} = \left(\frac{2\overline{D}}{q_0}\right)\left(\frac{dn}{d\epsilon_g}\right)_{q'_{eq}}. \tag{25}$$

It is important to note that the result in Eq. (23) is always negative, and in Eq. (24) is always positive, since D appears squared, and $(dn/d\epsilon_g)_{q'_{eq}}$ is negative.

The value of τ_I as a function of temperature is not known in Ti_2O_3. However, in studies of the magneto-electroacoustic effect in Bi, τ_I, which was shown to be dominated by phonon-assisted hole-electron interband scattering, dropped sharply as the temperature of the sample was raised, decreasing to $\sim 10^{-12}$ s at ~ 100 K.[30,31] This suggests that in Ti_2O_3 above 450 K, where the bands have crossed, the relaxation rate τ_I could be short enough so that Eqs. (23) and (24) could give non-negligible contributions. However, a relationship we derive in Sec. V between $(1/\tau_I)$ and an interband contribution to $(1/\tau_{el})$ after band crossing suggests that $\omega_0\tau_I$ in Ti_2O_3 is $\sim$4–6, making the contributions of Eqs. (23) and (24) small.

Even though the exact mechanism of phase transition in Ti_2O_3 is not established, the condition for equilibrium, Eq. (11), should still hold true. Therefore, neglecting the small corrections due to the η's, the relation between Δq_{eq} and n in Eq. (19) can be treated as an empirical one. An empirical estimate of Δq_{eq} for the A_{1g} mode as a function of T_L can be obtained for Ti_2O_3 from the changes observed in Ti-Ti pair distance as the temperature T_L is raised. This distance has been carefully measured in x-ray diffraction studies through the transition.[11] The measurements indicate that the Ti-Ti pair coordinates and the surrounding oxygen coordinates change in a manner qualitatively consistent with the behavior expected of the A_{1g} coordinate q [see Fig. 1(b)]. An approximate decomposition of the changes in coordinates through the transition can be made into c-axis strain and displacement q by comparing the fractional change in c-axis coordinate to the fractional change in Ti-Ti pair spacing. The latter change is about twice the former, suggesting that half the Ti-Ti displacement is due to the change in A_{1g} coordinate q.

To compare the measured Δq_{eq} as a function of T_L with Eq. (19), values of $2D$ and of n as a function of T_L must be obtained. Unfortunately, the value of $2\overline{D}=D_1-D_2$ is not known, although we obtain a value of $|D_2|\cong 2.0$ eV from comparison of a theoretical calculation of $1/\tau_{el}$ at room temperature with the measured value (see Sec. V). Furthermore, values of n are found experimentally to be roughly in the range of $\sim$3.9 to 5.9×10^{19} cm^{-3} at 300 K,[17] but values have not been reported at all at higher temperatures. To calculate n from a band model, the effective spherical constant energy surface band masses $(m_1^\star/m_0)$ and $(m_2^\star/m_0)$ of the conduction and valence bands must be known, as well as ϵ_g at each temperature T_L. A measurement of the effective mass for the valence band, $(m_2^\star/m_0)\cong 5$, has been obtained from early measurements of thermoelectric power,[15] and in fact this mass is used in Sec. V in determining the value of $|D_2|$.

To test Eq. (19), we must first obtain results for (n/n_0) as a function of temperature. If values of $(m_1^\star)$ and $(m_2^\star)$ for the conduction and valence bands and T_L are given, and the value of ϵ_g is known, then n can be calculated from the condition that at equilibrium, the number of electrons in intrinsic Ti_2O_3 equals the number of holes. This condition is

$$n = N_1\int_0^\infty \rho_1(\epsilon)\frac{d\epsilon}{e^{\beta(\epsilon+\epsilon_1-\epsilon_F)}+1}$$

$$= N_2\int_0^\infty \rho_2(\epsilon)\frac{d\epsilon}{e^{\beta(\epsilon-\epsilon_2+\epsilon_F)}+1}. \tag{26}$$

In Eq. (26), $\epsilon_g=\epsilon_1-\epsilon_2$, while N_1 and N_2 are the number of conduction and valence band edges, respectively, in the Brillouin zone. Band structure calculations indicate that $N_1=3$ and $N_2=2$.[19] The density of state factors in the effective mass approximation are given by

$$\rho(\epsilon) = C\epsilon^{1/2}, \tag{27}$$

where

$$C = \frac{8\pi\sqrt{2}}{h^3}(m^\star)^{3/2}. \tag{28}$$

When Eq. (26) is applied to the valence band of Ti_2O_3, we can write the expression for n, the number of holes per unit volume in the valence band as

$$n = 2.84\times 10^{19}\ \text{cm}^{-3}\times\left(\frac{m_2^\star}{m_0}\right)^{3/2}\left(\frac{T_L}{T_{RT}}\right)^{3/2}$$

$$\times N_2\int_0^\infty \frac{x^{1/2}dx}{e^{(x-\eta_2)}+1}, \tag{29}$$

where $\eta_2=\epsilon_{F_2}/k_BT_L$, $x=\epsilon/k_BT_L$, and ϵ_{F_2} is the Fermi level measured down from the top of the valence band (see Fig. 7). Equation (26) for given values of T_L, ϵ_g, and $(N_1/N_2)(m_1^\star/m_2^\star)^{3/2}$ allow a determination of both ϵ_F and n.

To make use of the x-ray data in testing Eq. (19), we evaluate the quantities

$$(\Delta q_{eq})_{T_L} \equiv [(q_{eq})_{T_L} - (q_{eq})_{300\,\text{K}}] \tag{30}$$

at the temperatures at which the x-ray data were taken.[11] As discussed above, we identify $(q_{eq})_{T_L}$ as approximately half of the Ti-Ti pair spacing from x-ray measurements at T_L. Assuming the effects of η_{e_1} and η_{h_2} are small at equilibrium, we then obtain from Eq. (19),

$$(\Delta q_{eq})_{T_L} = -\frac{1}{\omega_0^2\mu}\left(\frac{2\overline{D}}{q_0}\right)\frac{(\Delta n)_{T_L}}{n_0}, \tag{31}$$

where $(\Delta n)_{T_L}\equiv[(n)_{T_L}-(n)_{300\,\text{K}}]$. While $\overline{D}$ may change by $\sim$15% or so as the temperature rises through the soft transition, as do elastic constants, n will change by over an order of magnitude. For simplicity, we will then treat $\overline{D}$ as a constant.

The strategy for testing the reasonableness of Eq. (19) is to take (m_2^*/m_0) as 5 (the value used in Sec. V to obtain $|D_2|$), $N_2=2$, $N_1=3$, and then to choose a value of $\rho^{3/2}$ defined as

TABLE I. Model band parameters deduced from x-ray data on Ti_2O_3, using $(m_2^\star/m_0)=5$ and values of $\rho^{3/2}\equiv(N_1/N_2)(m_1^\star/m_2^\star)^{3/2}$ shown. Values of ϵ_g at $T=300$ and at 450 K are, respectively, taken as $\epsilon_g=0.15$ eV and $\epsilon_g=0$. Results for n(390 K), n(490 K), and n(565 K) have also been calculated, but are not included for lack of space. Negative values of ϵ_g correspond to overlapping bands.

$\rho^{3/2}$	ϵ_g(390 K) eV	ϵ_g(490 K) eV	ϵ_g(565 K) eV	ϵ_g(621 K) eV	n(300 K) $\times10^{-19}$ cm^{-3}	n(450 K) $\times10^{-19}$ cm^{-3}	n(621 K) $\times10^{-19}$ cm^{-3}	$(2\overline{D})$ eV	ϵ_{F_2}(621 K) eV
1	0.095	-0.034	-0.054	-0.061	2.76	79.06	199.8	-6.50	0.030
1.5	0.098	-0.034	-0.055	-0.062	3.36	144.60	363.4	-3.50	0.046
2	0.100	-0.035	-0.056	-0.063	3.90	221.21	563.1	-2.28	0.057
2.5	0.101	-0.035	-0.056	-0.064	4.42	305.98	788.0	-1.64	0.065
3	0.102	-0.036	-0.057	-0.065	4.76	398.69	1006.3	-1.26	0.073
4	0.104	-0.036	-0.058	-0.066	5.48	608.25	1567.2	-0.82	0.084
5	0.105	-0.037	-0.059	-0.067	6.24	828.02	2085.7	-0.60	0.093

$$\rho^{3/2}\equiv(N_1/N_2)(m_1^*/m_2^*)^{3/2}. \tag{32}$$

With these choices, n can be obtained at $T_L=300$ K (where $\epsilon_g=0.15$ eV) and at $T_L=450$ K (where $\epsilon_g\cong0$). Applying Eq. (31) for $T_L=450$ K, with the values $\omega_0=233$ cm^{-1} in wave number units, $\mu\sim24$ (the Ti_2O_3 reduced mass in molecular weight units), $q_0=2.6$ Å , and $1/n_0=51.8$ Å ^{3}, we then obtain a value for $2D$. Next, applying Eq. (31) to the x-ray data at other temperatures T_L, we can calculate $(\Delta n)_{T_L}$ from the ratio

$$\frac{(\Delta n)_{T_L}}{(\Delta n)_{450\,\mathrm{K}}}=\frac{(\Delta q_{\mathrm{eq}})_{T_L}}{(\Delta q_{\mathrm{eq}})_{450\,\mathrm{K}}}. \tag{33}$$

Finally, ϵ_g at the temperature T_L is determined from $(\Delta n)_{T_L}$.

This procedure was followed for a number of values of $\rho^{3/2}$ using tables of Fermi integrals.[32] The results obtained for $(2\overline{D})$, and for n and ϵ_g at a number of temperatures T_L are shown in Table I. Negative values of ϵ_g refer to values of band crossing. We see that reasonable results are obtained for $(n)_{(300\,\mathrm{K})}$ and for $(2\overline{D})$ for values of $\rho^{3/2}$ of ~1.5–3. The choice of $(m_2^*/m_0)=5$ was made somewhat arbitrarily in order to have only one variable to consider. This mass is no better established than other parameters in Ti_2O_3. Transport measurements and band structure calculations suggest that (m_1^*/m_2^*) should be greater than 1. It should be noted that changing (m_2^*/m_0) changes n and $2D$, which scale, respectively, as $(m_2^*/m_0)^{3/2}$ and $(m_2^*/m_0)^{-3/2}$. But the choice of (m_2^*/m_0) does not affect ϵ_g values, which depend only on $\rho^{3/2}$. Remarkably, the values of ϵ_g at different temperatures vary only slightly with $\rho^{3/2}$ in the range studied, and all of these values lead to an overlap of the valence and conduction band after the soft transition of about 0.06 eV. A rough value of the position of the Fermi level in the valence band at $T_L=621$ K for $\rho^{3/2}\sim2$ is $\epsilon_{F_2}\sim0.06$ eV. The values of ϵ_g at several temperatures obtained by this method for $(m_2^*/m_0)=5$ and $\rho^{3/2}=2$ are plotted vs T_L as an inset in Fig. 6.

As pointed out earlier, we have extended the interpretation of Eqs. (19)–(22) to include both the effects of charge redistribution and thermodynamic balance between core energy and deformation potential energy. It should be noted that, although some contribution of charge redistribution might be included in explaining the experimental results of Δq_{eq} with T_L, the value of $2D$ obtained in Table I for $\rho^{3/2}$ about equal to 2 is quite reasonably interpreted as a deformation potential.

Having considered the case of equilibrium at a temperature T_L (that is, for both lattice and electron system at temperature T_L), we now consider the changes introduced by the incidence of the pump pulse. Assuming most of the DECP signal observed is due to transfer of electrons out of the valence band (2) and into some excited bands labeled by (i), we write from Eq. (19) the change in δq_{eq} produced by the pump,

$$\delta q_{\mathrm{eq}}\cong\frac{1}{\omega_0^2\mu}\left[\left(\frac{\delta n}{n_0}\right)\left(\frac{D_2-D_i}{q_0}\right)-\left(\frac{\delta n}{n_0}\right)\left(\frac{D_i}{q_0}\right)\eta_{e_i}+\left(\frac{n+\delta n}{n_0}\right)\left(\frac{D_2}{q_0}\right)\Delta\eta_{h_2}+\left(\frac{\delta n}{n_0}\right)\left(\frac{D_2}{q_0}\right)\eta_{h_2}^{(0)}\right], \tag{34}$$

where δn is the number of electrons transferred, D_i is an effective deformation potential for the excited bands (i), η_{e_i} represents the correction due to the distribution of electrons in the bands (i), $\eta_{h_2}^{(0)}$ is the value of η_{h_2} before the pump pulse, and $\Delta\eta_{h_2}\equiv(\eta_{h_2}-\eta_{h_2}^{(0)})$ is the change produced by the pump pulse. Before band overlap ($T_L<450$ K), the only rapidly varying quantities (on a time scale of ~1 ps) are η_{e_i} and $\Delta\eta_{h_2}$. These two parameters can change rapidly due to the cooling of the excited electron distribution through the mechanism of the electron-phonon interaction (see Sec. V). δn will change much more slowly by interband recombination processes. In addition, the effective D_i may change slowly as the electrons transfer between higher-lying bands. After band crossing ($T_L>450$ K), there will be a rapidly changing interband contribution to δq_{eq} produced by the decay of δn due to interband recombination (see Sec. V).

We will estimate the size of the displacement δq of the A_{1g} mode produced by the pump pulse in our DECP experiments in Ti_2O_3, by establishing a rough calibrating relationship between measured values of $\Delta R/R$ and the displacements producing them. This can be done in an approximate manner by comparing the change in reflectivity in raising the sample temperature T_L from 300 K to 450 K, to the corresponding change in equilibrium Ti-Ti pair spacing.[8]

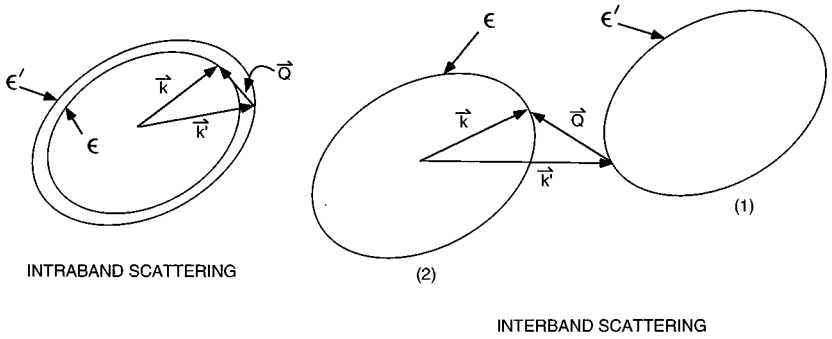

FIG. 8. A schematic picture of the electron intraband and interband scattering diagram with emission of phonons in Ti_2O_3.

The reflectivity is found to decrease by $\sim 10\%$ during this increase in temperature, while the Ti-Ti pair spacing increases by about 0.04 Å. We assume that $(\Delta R/R)$, produced by changes in Ti-Ti pair spacing, is roughly proportional to those changes, whether produced by changes in c-axis strain or by changes in $A_{1g\swarrow}$ coordinate. If this proportionality holds approximately whether or not the pair spacing changes have their equilibrium values, then we can establish our calibration. The result is

$$\delta q \cong \frac{0.04}{(-0.10)}\left(\frac{\Delta R}{R}\right)\text{Å} \cong -0.40\left(\frac{\Delta R}{R}\right)\text{Å}. \tag{35}$$

It should be noted that this calibration applies only to that portion of $\Delta R/R$ which is due to changes in displacement of the $A_{1g\swarrow}$ coordinate, and thus does not apply to the A term in Eq. (1).

To apply Eq. (35) to Ti_2O_3 at room temperature, we note that B, which is equal to -5.7×10^{-2}, is the value of $\Delta R/R$ due to $\delta q_{\rm eq}$ at $t=0^+$. This yields

$$\delta q_{\rm eq}(t=0^+) \cong 0.023 \text{ Å}. \tag{36}$$

The total swing in δq in the first cycle of vibration is thus $\delta q \cong 0.046$ Å. This is to be compared with the value of the zero point r.m.s. amplitude of the $A_{1g\swarrow}$ phonon,

$$\overline{q} = \sqrt{\frac{\hbar}{2\mu\omega_0}} = \frac{3.98}{[\mu(MW)\times\lambda^{-1}(\text{cm}^{-1})]^{1/2}} \text{ Å}, \tag{37}$$

in convenient units. Taking $\mu \sim 24$ in molecular weight units, and the $A_{1g\swarrow}$ mode frequency as 233 cm^{-1}, we find

$$\overline{q} \cong 0.053 \text{ Å}. \tag{38}$$

V. ELECTRON RELAXATION

As shown in Fig. 6, the behavior of the effective relaxation rate $1/\tau_{\rm el}$ with sample temperature indicates a strong correlation with the disappearance of the energy gap. While there may be other ways of understanding this result, the behavior strongly suggests that the background decay for times less than a few ps is associated in some way with carrier distributions in bands (1) and (2). Our model of the pump excitation process in Ti_2O_3 will assume that the spectra produced in the first few picoseconds after the arrival of the pulse are due mainly to the excitation of carriers from the valence band (2), leaving the valence band electrons, after rapid equilibration, at a temperature $T_{\rm el}$. The pump pulse in our present experiments removes electrons from the valence band at a depth of a fraction of a volt, adding considerable energy, but changing the number of carriers by only a small amount. The decay of this excess energy is mainly due to carrier scattering, with the emission or absorption of phonons. Before band crossing, the relaxation rate $1/\tau_{\rm el}$ would be mainly due to an intraband contribution

$$\frac{1}{\tau_{\rm el}} = \frac{1}{\tau_{\rm el\ intra}}. \tag{39}$$

After band crossing, however, there would be an interband contribution as well, so that,

$$\frac{1}{\tau_{\rm el}} = \frac{1}{\tau_{\rm el\ intra}} + \frac{1}{\tau_{\rm el\ inter}}. \tag{40}$$

Both of these components would depend on the energy gap ϵ_g (which varies with lattice temperature T_L), as well as the effective electron temperature $T_{\rm el}$.

Questions have been raised[28] concerning the correctness of describing excited electron distributions in optical pump-probe experiments in terms of an effective electron temperature $T_{\rm el}$. However, it is difficult to attempt any analysis on a more general basis, and theoretical calculations based on this model yield results which are reasonably consistent with the observation of relaxation rates in Ti_2O_3 over a range of lattice temperatures T_L.

Allen[33] has presented a theoretical description of the cooling of a heated electron gas raised to a temperature $T_{\rm el}$ by an exciting optical pulse, and this theory has proven to be particularly useful in describing femtosecond pump-probe experiments in metals. We will adapt his treatment to the more general case of a material that does not have a sharply defined Fermi surface, as in the case of Ti_2O_3 at room temperature.

Allen's discussion begins with an expression for the rate of energy loss due to exchange of energy between two groups of electrons, labeled by $\vec{k}$ and $\vec{k}'$ which have been heated by a pump pulse (see Fig. 8). Allen's original treatment deals with these heated electrons in the same band, but we will generalize the result to the case where $\vec{k}$ and $\vec{k}'$ may not be in the same band. Transitions occur between these two groups by phonon emission and absorption processes, with the phonon population at equilibrium at a temperature T_L.

For the set of electrons $\vec{k}$ and $\vec{k}'$ heated to a common temperature $T_{\rm el}$, the rate of energy loss can be written

$$\frac{\partial E}{\partial t}=\Sigma_{k,k',Q}\left(\frac{2\pi}{\hbar}\right)|M_{k,k'}|^2(\hbar\omega_Q)[(f_{k'}-f_k)n_Q(T_L) - f_k(1-f_{k'})]\delta(\epsilon_k-\epsilon_{k'}-\hbar\omega_Q)\delta(\vec{k}-\vec{k'}-\vec{Q}). \tag{41}$$

Here, k labels an initial electron state of energy ϵ_k; k' labels a final electron state of energy $\epsilon_{k'}$; Q labels a phonon of wave vector $\vec{Q}$, and energy $\hbar\omega_Q$. $M_{k,k'}$ is a matrix element for the scattering from the state k to k' with the emission or absorption of a phonon. f_k and $f_{k'}$ are the Fermi distribution functions for excited electrons at temperature $T_{\rm el}$; and $n_Q(T_L)$ is the Bose distribution function for phonons at temperature T_L,

$$n_Q(T_L)=[e^{\hbar\omega_Q/k_BT_L}-1]^{-1}. \tag{42}$$

In general, $T_{\rm el}$ will decrease and T_L will increase as a function of time after the pump pulse. We assume that the change in T_L is small and can be neglected. The δ functions in Eq. (41) guarantee energy and wave vector conservation in the phonon emission and absorption processes. It should be noted that if there are several electronic bands involved in the electron cooling, there may be intraband and interband contributions to Eq. (41) from each band, and if a number of phonon modes are involved, there will be a contribution from each one.

Equation (41) can be simplified somewhat by using the fact that the rate of loss of electron energy vanishes if the phonon system is at the electron temperature $T_{\rm el}$. Equation (41) can then be written

$$\frac{\partial E}{\partial t}=-\Sigma_{k,k',Q}\left(\frac{2\pi}{\hbar}\right)|M_{k,k'}|^2(\hbar\omega_Q)(f_{k'}-f_k)[n_Q(T_{\rm el}) - n_Q(T_L)]\delta(\epsilon_k-\epsilon_{k'}-\hbar\omega_Q)\delta(\vec{k}-\vec{k'}-\vec{Q}), \tag{43}$$

where $n_Q(T_L)$ and $n_Q(T_{\rm el})$ are the phonon populations at temperatures T_L and $T_{\rm el}$, respectively.

For simplicity, we next make the assumption that the relevant values of $\hbar\omega_Q$ in Eq. (43) are less than the excited electron energy $\simeq k_BT_{\rm el}$, so that it is reasonable to expand $f_{k'}$ as

$$f_{k'}\simeq f_k+\left(\frac{\partial f}{\partial\epsilon}\right)_k(-\hbar\omega_Q). \tag{44}$$

This is roughly the case for Ti_2O_3 even if the major phonon involved is, as we will argue, the A_{1g} optical phonon at a frequency of $\sim 233\ {\rm cm}^{-1}$. Using Eq. (44), and changing from summation to integration in Eq. (43), we can write

$$\frac{\partial E}{\partial t}=-\tfrac{1}{2}V^2\int\int P(\epsilon,\epsilon')\left(-\frac{\partial f}{\partial\epsilon}\right)\rho_2(\epsilon')d\epsilon'\rho_1(\epsilon)d\epsilon, \tag{45}$$

where $\rho_2(\epsilon)$ and $\rho_1(\epsilon')$ are, respectively, the densities of states in energy on the constant energy surfaces containing the states $\vec{k}$ and $\vec{k'}$ (see Fig. 8). The factor V^2 comes from the proportionality of the density of states to the sample volume. The factor of 1/2 in Eq. (45) comes from electron spin conservation during scattering. $P(\epsilon,\epsilon')$ represents an average over the two constant energy surfaces of the energy loss rate,

$$P(\epsilon,\epsilon')=\left\langle\left(\frac{2\pi}{\hbar}\right)\Sigma_Q|M_{k,k'}|^2(\hbar\omega_Q)^2[n_Q(T_{\rm el})-n_Q(T_L)] \times\delta(\epsilon_k-\epsilon_{k'}-\hbar\omega_Q)\delta(\vec{k}-\vec{k'}-\vec{Q})\right\rangle_{\rm av}. \tag{46}$$

As we will see in a moment, $\rho_1(\epsilon')$ in Eq. (45) may refer to a different band, implying interband scattering, but only if the distributions in the two bands are characterized by a common $T_{\rm el}$. For the moment we consider intraband scattering only. For energy loss by *acoustic* phonons, not every point on the surface with energy ϵ' may be accessible to a given point on the surface with energy ϵ by a phonon process consistent with the two delta functions in Eq. (46). For energy loss due to *optical* phonons we can describe the phonon by an average flat spectrum of angular frequency ω_0, independent of $\vec{Q}$, so that all points on the energy surface ϵ' at energy $\epsilon+\hbar\omega$ are accessible to the scattering process. For an optical phonon, neglecting the Q dependence of the matrix element, calling $\rho_2(\epsilon)=\rho(\epsilon)$, and replacing $\rho_1(\epsilon')$ by $\rho(\epsilon+\hbar\omega)\simeq\rho(\epsilon)$, the integration over ϵ' in Eq. (45) can be performed to yield

$$\frac{\partial E}{\partial t}=-\tfrac{1}{2}V^2\left(\frac{2\pi}{\hbar}\right)|M|^2(\hbar\omega_0)^2[n(T_{\rm el})-n(T_L)] \times\left[\int\left(-\frac{\partial f}{\partial\epsilon}\right)[\rho(\epsilon)]^2d\epsilon\right]_{T_{\rm el}}. \tag{47}$$

We have introduced the bracket $[]_{T_{\rm el}}$ as a reminder that the integral in Eq. (47) is taken with $f(\epsilon)$ evaluated at $T=T_{\rm el}$.

From Eq. (47), we can define approximately a relaxation rate $(1/\tau_{\rm el\ intra})$, which describes the initial rate of decay of energy of the excited electron gas after the pump pulse by the relation

$$\left(\frac{1}{\tau_{\rm el\ intra}}\right)\simeq-\frac{1}{\Delta E}\frac{\partial E}{\partial t}. \tag{48}$$

In using this definition of $1/\tau_{\rm el}$, we are assuming that the disturbance in carrier energy ΔE is the measure of the electronic excitations n^* in Eq. (4). Combining Eqs. (47) and (48), we have

$$\left(\frac{1}{\tau_{\rm el\ intra}}\right)=\frac{1}{2}\left(\frac{2\pi}{\hbar}\right)V|M|^2_{\rm intra}(\hbar\omega_0)^2[n(T_{\rm el})-n(T_L)] \times\frac{\left[\int\left(-\frac{\partial f}{\partial\epsilon}\right)[\rho(\epsilon)]^2d\epsilon\right]_{T_{\rm el}}}{\left[\int\epsilon f(\epsilon)\rho(\epsilon)d\epsilon\right]_{T_{\rm el}}-\left[\int\epsilon f(\epsilon)\rho(\epsilon)d\epsilon\right]_{T_L}}, \tag{49}$$

where ΔE is V times the denominator in Eq. (49).

Because the A_{1g} mode in Ti_2O_3 appears to strongly modulate the energy gap, and therefore appears to be strongly coupled to the valence band (2) and conduction band (1), we focus our attention on this mode as the one dominating the relaxation in Eq. (47). It should be kept in mind that this is an approximation, and that some contribution from other vibrational modes could be significant. Acoustic mode intraband scattering is likely to be small, since acoustic mode scattering is proportional to $|Q|^2$,[34] which should be small for scattering near a band edge. On the other hand, for interband scattering across the Brillouin zone, both optical and acoustic modes have been found to be important, depending on sample temperature.[30,31] The application of Eq. (47) to interband scattering would be appropriate only if the carrier distribution in both initial and final bands were characterized by a common temperature $T_{\rm el}$.

Assuming that the matrix element describing the electron-phonon coupling to the A_{1g} mode can be expressed in terms of a deformation potential, $|M|^2_{\rm intra}$ can be written[34]

$$|M|^2_{\rm intra}=\left(\frac{v_{\rm uc}}{V}\right)\overline{q^2}\left(\frac{\partial u}{\partial q}\right)^2. \tag{50}$$

In Eq. (50), $(\partial u/\partial q)$ represents the modulation in energy of the band edge with A_{1g} mode displacement q, $v_{\rm uc}\equiv 1/n_0$ is the volume of the unit cell, and $\overline{q}$ is the zero-point root mean square displacement of the phonon, given by Eq. (37).

Equation (50) can be written in terms of a deformation potential D as defined in Eq. (7). We take $[\rho(\epsilon)]$ as a spherical band density of states given by Eq. (27). It is convenient to write the integrals in Eq. (49) in dimensionless units, and to regroup the terms.

We then have

$$\left(\frac{1}{\tau_{\rm el\ intra}}\right)=\left[\frac{(m_0)^{3/2}}{\sqrt{2}\pi\hbar^2(k_BT_{RT})^{1/2}}\right]\times\left[D^2\left(\frac{m^*}{m_0}\right)^{3/2}\left(\frac{v_{\rm uc}}{q_0^2}\right)\frac{1}{\mu}\right]\times P\times S, \tag{51}$$

where

$$P\equiv\left(\frac{\hbar\omega_0}{k_BT_{\rm el}}\right)n(T_{\rm el})\left[1-\frac{n(T_L)}{n(T_{\rm el})}\right], \tag{52}$$

$$S\equiv\left(\frac{T_{\rm RT}}{T_{\rm el}}\right)^{1/2}\frac{[\int_0^\infty f dx]_{T_{\rm el}}}{\left[\int_0^\infty fx^{3/2}dx\right]_{T_{\rm el}}-(T_L/T_{\rm el})^{5/2}\left[\int_0^\infty fx^{3/2}dx\right]_{T_L}}, \tag{53}$$

and the Fermi function $f(x)$ is of the form

$$f(x)=[e^{(x-\epsilon_F/kT)}+1]^{-1}. \tag{54}$$

In Eq. (51), the first bracketed factor contains parameters which are independent of temperature and material. $k_BT_{\rm RT}$ is the value of k_BT at room temperature, $T_{\rm RT}=300$ K. The second bracketed factor contains material-dependent but temperature independent parameters. The term P is a dimensionless phonon occupation factor which is usually of the order of unity for $(\hbar\omega_0/k_BT_{\rm el})\ll 1$, since in that limit $n(T_{\rm el})\simeq(k_BT_{\rm el}/\hbar\omega_0)$. The last, dimensionless, temperature-dependent statistical factor S depends on the value of the parameters $\epsilon_F(T_{\rm el})/k_BT_{\rm el}$ and $\epsilon_F(T_L)/k_BT_L$. The term $[\int_0^\infty f dx]_{T_{\rm el}}$ in S was obtained by partial integration of $[\int_0^\infty(-\partial f/\partial x)x dx]_{T_{\rm el}}$. Rewriting Eq. (51) in terms of parameters expressed in convenient units, we find

$$\left(\frac{1}{\tau_{\rm el\ intra}}\right)=0.453\times10^{12}\ \ {\rm s}^{-1}\times\left[D^2({\rm eV}^2)\left(\frac{m^*}{m_0}\right)^{3/2}\times\left(\frac{v_{\rm uc}(\text{Å}^3)}{q_0^2(\text{Å}^2)}\right)\frac{1}{\mu(MW)}\right]\times P\times S. \tag{55}$$

In Eq. (55), the reduced mass μ is expressed in molecular weight units. It should be noted that the dependence of $(1/\tau_{\rm el\ intra})$ on the dominant optical phonon is represented only in the values of D, q_0, the appropriate value of μ, and in the factor P. Equation (55) should apply to the case of Ti_2O_3, at least in the temperature range from 300 K to $\sim$450 K, where $(1/\tau_{\rm el\ inter})$ should be negligible.

To apply Eq. (55) to Ti_2O_3, we must then evaluate the bracketed, temperature independent factor, along with the factors P and S, which depend on $T_{\rm el}$, T_L, and the ratio ϵ_{F2}/k_BT at these temperatures. We have evaluated P and S and their product for many combinations of parameters, over a range of values of T_L from 300 K to $\sim$450 K, where the band gap vanishes and for values of $T_{\rm el}-T_L$ from 50 K to several hundred K. Over this range of parameter value combinations, the product PS was nearly constant at a value of $\sim 0.5\pm 15\%$. The reason for this constancy can be at least partly understood by noting that the PS product is proportional to $\sim(1/\Delta E)\times[n(T_{\rm el})-n(T_L)]$. An increase in $T_{\rm el}$ thus increases ΔE, but also produces a compensating increase in $[n(T_{\rm el})-n(T_L)]$. The constancy of the product PS implies that $1/\tau_{\rm el}$ should be nearly constant with increasing T_L as the temperature approaches 450 K, where band crossing begins. This prediction is consistent with observation.

We can apply Eq. (55) to the relaxation rate observed in Ti_2O_3 at 300 K, using the value $PS\cong 0.5$. The effective mass μ of the vibrating atoms in the A_{1g} mode of Ti_2O_3 is approximately the reduced mass of the vibrating Ti atom pair, $\mu\cong 24$; the unit cell volume $v_{\rm uc}$ is 51.8 Å^3; and q_0, taken as the distance between Ti atoms in a vibrating pair, is 2.6 Å. The carrier effective mass ratio for the valence band is not conclusively known, but one value quoted in the literature[15] is $(m^*/m_0)=5$. The remaining unknown parameter is D_2 for the valence band, but this can be determined by equating the observed relaxation rate at room temperature $(1/\tau_{\rm el}=3.3\times10^{12}\ {\rm s}^{-1})$ to Eq. (55). The result is, $|D_2|\cong 2.0$ eV. It should be kept in mind that the value of $(m_2^\star/m_0)=5$ is not well established. Thus, the value of $|D_2|$ determined from our experiment will scale as $(m_2^\star/m_0)^{-3/4}$.

We now turn our attention to the consideration of $1/\tau_{\rm el}$ after the bands cross. Equation (55) can still be used to describe the electron *intraband* relaxation rate, after band crossing, and we first ask what combination of ϵ_{F2} and $T_{\rm el}$ is

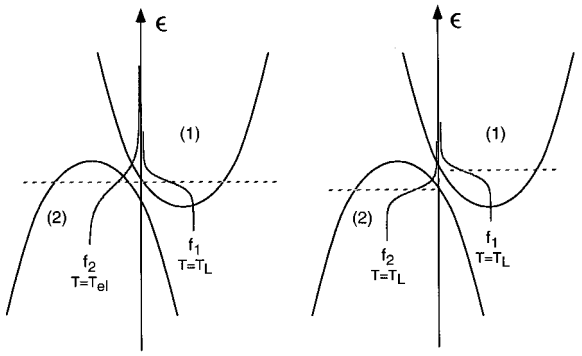

FIG. 9. A schematic diagram showing the electron populations representing $(1/\tau_{\text{el inter}})_b$ (to the left) and $1/\tau_I$ in Ti_2O_3 (see text, Sec. V). The figures show Fermi distributions as a function of energy. For $(1/\tau_{\text{el inter}})_b$ the Fermi levels nearly coincide, but the temperature T_{el} in band (2) is greater than T_L in band (1). For $1/\tau_I$ the Fermi levels are shifted, and the temperatures T_L in both bands are the same.

required in order to explain the measured value of relaxation rate at $T_L \cong 600$ K on the basis of intraband relaxation alone. We noted in Sec. IV that based on the thermodynamic model considered, the equilibrium value of $|\epsilon_g|$ at $T_L = 621$ K was about 0.06 eV, and the value of ϵ_{F2} was roughly the same. We find that values of ϵ_{F2} much larger than 0.06 eV (which would have to be produced by the pump pulse) must be assumed to give relaxation rates at $T_L = 600$ K that are three times those at 300 K. The number of carriers n required to produce this large shift in ϵ_{F2} is found to be over an order of magnitude larger than the total value of δn produced by the pump pulse. Thus, an increase in intraband scattering after the bands cross can only be a small part of the explanation for the factor of 3 increase observed in $(1/\tau_{\text{el}})$.

To compute the *interband* contribution to $1/\tau_{\text{el}}$ when the bands have crossed, we return to Allen's treatment of the two sets of electrons labeled by $\vec{k}$ and $\vec{k}'$, which are interacting by the emission and absorption of phonons of angular frequency ω_0. We will assume that the label $\vec{k}$ refers to electrons in band (2) and $\vec{k}'$ to electrons in band (1). We consider two possibilities.

Case (a): Carriers in both bands (2) and (1) are raised to temperature $\sim T_{\text{el}}$ by the pump pulse.

Case (b): Only the carriers in valence band (2) are heated by the pump pulse to temperature T_{el}, while carriers in conduction band (1) remain at essentially T_L.

For case (a), Eq. (43) applies, which means that the final result for $(1/\tau_{\text{el inter}})_a$ is of the same form as Eq. (49), except that the integral in the numerator involves the joint density of states $\rho_1(\epsilon)\rho_2(\epsilon)$ for the two bands, and the denominator has a contribution to ΔE from both bands. However, the result will be proportional to an interband matrix element $|M|^2_{\text{inter}}$ which should in general be different from $|M|^2_{\text{intra}}$. The density of states factor in the numerator of Eq. (49) would increase, but this would be largely compensated by an increase in ΔE. Therefore, except in the unlikely case that $|M|^2_{\text{inter}} \gg |M|^2_{\text{intra}}$, $(1/\tau_{\text{el inter}})_a$ cannot explain the large increase in $(1/\tau_{\text{el}})$ after band crossing.

To evaluate the result for case (b), we generalize Allen's expression[33] for the rate of energy loss of two groups of electrons labeled by $\vec{k}$ and $\vec{k}'$ and interacting by the emission and absorption of phonons. $\vec{k}$ labels the electrons in band (2) at temperature T_{el}, while $\vec{k}'$ labels the electrons in band (1) at temperature T_L. Since the electrons in the two bands are not at the same temperature, we cannot apply Eq. (43) to this case (see Fig. 9). In the simplest situation, Fig. 9 corresponds to cooling by exchanging hot electrons in band (2) for cooler electrons in band (1) by scattering via phonon emission and absorption. Of course, if the difference in temperature between the electrons in these two bands vanishes, then the large contribution from case (b) vanishes, and we are left with the smaller contribution from case (a).

The general expression for $(1/\tau_{\text{el inter}})_b$ can be written

$$\left(\frac{1}{\tau_{\text{el inter}}}\right)_b = \frac{1}{2}\left(\frac{2\pi}{\hbar}\right)|M|^2_{\text{inter}}(k_B T_{\text{RT}})^{1/2} \times \frac{V N_1 N_2 C_1 C_2 I_{T_{\text{el}},T_L}}{N_2 C_2 \Delta E'}, \tag{56}$$

where

$$I_{T_{\text{el}},T_L} = \left(\frac{1}{k_B T_{\text{RT}}}\right)^3 \left[\int_0^{\epsilon_g + \hbar\omega_0} \{ n f_2(\epsilon)[1 - f_1(\epsilon - \hbar\omega_0)] - (n+1) f_1(\epsilon - \hbar\omega_0)[1 - f_2(\epsilon)] \} \times (\epsilon)\epsilon^{1/2} \times (|\epsilon_g| - \epsilon + \hbar\omega_0)^{1/2} d\epsilon \right.$$
$$\left. + \int_0^{\epsilon_g - \hbar\omega_0} \{ (n+1) f_2(\epsilon) \times [1 - f_1(\epsilon + \hbar\omega_0)] - n f_1(\epsilon + \hbar\omega_0)[1 - f_2(\epsilon)] \} \times (\epsilon)\epsilon^{1/2} (|\epsilon_g| - \epsilon - \hbar\omega_0)^{1/2} d\epsilon \right], \tag{57}$$

and

$$\Delta E' = \frac{\Delta E}{N_2 C_2 (k_B T_{\text{RT}})^{5/2}} = \left(\frac{1}{k_B T_{\text{RT}}}\right)^{5/2} \left[\left\{ \int_0^\infty [1 - f_2(\epsilon)](\epsilon)\epsilon^{1/2} d\epsilon \right\}_{T_{\text{el}}} - \left\{ \int_0^\infty [1 - f_2(\epsilon)](\epsilon)\epsilon^{1/2} d\epsilon \right\}_{T_L} \right]. \tag{58}$$

In Eq. (56), C_1 and C_2 are, respectively, the density of states factors given by Eq. (28) for the bands (1) and (2). $I_{T_{\rm el},T_L}$ and $\Delta E'$ are dimensionless quantities. n is the phonon population factor at temperature T_L. The energy in the integrals is measured down from the top of band (2). The Fermi functions in Eq. (57) are given by

$$f_2(\epsilon)=\frac{1}{e^{(-\epsilon+\epsilon_{F_2'})/kT_{\rm el}}+1}, \tag{59}$$

$$f_1(\epsilon)=\frac{1}{e^{(-\epsilon+\epsilon_{F_2})/kT_L}+1}, \tag{60}$$

where ϵ_{F_2} is the Fermi level in both bands at T_L, and ϵ'_{F_2} is the Fermi level in band (2) at electron temperature $T_{\rm el}$. Although the schematic in Fig. 9 does not show a difference, the Fermi level ϵ'_{F_2} is not exactly the same as ϵ_{F_2}; ϵ'_{F_2} is calculated at temperatures $T_{\rm el}$ by the condition that the number of carriers is approximately the same as at temperature T_L before the pulse. In Eqs. (58), $f_2(\epsilon)$ is given by Eq. (59) in the first integral, and is the same as $f_1(\epsilon)$, Eq. (60) in the second integral.

We will apply Eq. (56) to the case of Ti_2O_3 after band crossing. To do the calculation realistically, we keep the dependence on $\hbar\omega_0$, which means that there will be a contribution to interband scattering with the absorption of a phonon even when a gap $\epsilon_g<\hbar\omega_0$ exists between valence and conduction band. We have performed the numerical integration of $I_{T_{\rm el},T_L}$ at temperatures $T_L=565$, 490, and 450 K using values of the gap given in Table I for the case $\rho^{3/2}=2$. With the assumption that the energy ΔE given to the valence band by the pump pulse is nearly constant at all temperatures, the denominator in Eq. (56) is constant and all of the dependence of $(1/\tau_{\rm el\ inter})_b$ on T_L is contained in $I_{T_{\rm el},T_L}$. For a given value of $T_{\rm el}$ at $T_L=565$ K the values of $T_{\rm el}$ are determined at other lattice temperatures by the condition that ΔE is constant. We have calculated $I_{T_{\rm el},T_L}$ at the three lattice temperatures assuming a value for $T_{\rm el}$ at $T_L=565$ K. Matching the measured value of $(1/\tau_{\rm el})$ at 565 K to the expression

$$\left(\frac{1}{\tau_{\rm el}}\right)=\left(\frac{1}{\tau_{\rm el\ intra}}\right)+KI_{T_{\rm el},T_L},$$

yields predicted values of $(1/\tau_{\rm el})$ at the temperatures $T_L=490$ and 450 K. Such calculations have been performed for $T_{\rm el}=665$ and 765 K at $T_L=565$ K, giving values of $\Delta E'=1.68$ and $\Delta E'=3.40$, respectively. For the case $\Delta E'=1.68$, we obtain $[I_{T_{\rm el},T_L}]_{565\ \rm K}=0.558$, $[I_{T_{\rm el},T_L}]_{490\ \rm K}=0.323$, and $[I_{T_{\rm el},T_L}]_{450\ \rm K}=0.052$. For $\Delta E'=3.40$, we find $[I_{T_{\rm el},T_L}]_{565\ \rm K}=1.03$, $[I_{T_{\rm el},T_L}]_{490\ \rm K}=0.564$, and $[I_{T_{\rm el},T_L}]_{450\ \rm K}=0.081$. These calculations yield the points shown in Fig. 6. The results for the two choices of $T_{\rm el}$ are only slightly different, and match the observed data reasonably well.

From Ref. 2, we can calculate the total energy per unit volume delivered by the pump pulse at the sample surface for 2 eV photons with the relation,

$$\Delta E_{\rm tot}({\rm eV\ cm^{-3}})=2.0\times10^{20}n_2(1-R)\ {\rm cm^{-3}}\times 2\ {\rm eV}, \tag{61}$$

where n_2 is the imaginary part of the index of refraction and R is the material reflectivity, both evaluated at the pump frequency. For Ti_2O_3 at room temperature, $n_2\cong 2$ and $R\cong 0.1$.[27] This yields $\Delta E_{\rm tot}\cong 7.2\times10^{20}$ eV cm^{-3}. Comparing the energy $\Delta E_{\rm tot}$ delivered to the sample by the pump pulse with ΔE corresponding to $T_{\rm el}=665$ and 765 K at $T_L=565$ K, we find ΔE is, respectively, 3.7% and 7.5% of $\Delta E_{\rm tot}$ for the two cases.

We will compare $(1/\tau_{\rm el\ inter})_b$ at 565 K given by Eq. (56), with $(1/\tau_{\rm el\ intra})$ at 300 K from Eq. (49). From the definitions of P and S in Eqs. (52) and (53), we can rewrite Eq. (49) as

$$\left(\frac{1}{\tau_{\rm el\ intra}}\right)=\frac{1}{2}\left(\frac{2\pi}{\hbar}\right)|M|^2_{\rm intra}V\times\frac{C_2(\hbar\omega_0)}{(k_BT_{RT})^{1/2}}\times PS. \tag{62}$$

Since $PS\sim 0.5$ at 300 K, we find

$$\frac{[(1/\tau_{\rm el\ inter})_b]_{565\ \rm K}}{[(1/\tau_{\rm el\ intra})]_{300\ \rm K}}=\frac{|M|^2_{\rm inter}}{|M|^2_{\rm intra}}N_2\left(\frac{N_1}{N_2}\right)\left(\frac{m_1^\star}{m_2^\star}\right)^{3/2}\times\frac{(k_BT_{\rm RT})}{(\hbar\omega_0)0.5}\frac{I_{T_{\rm el},T_L}}{\Delta E'}. \tag{63}$$

If we attribute the difference between $1/\tau_{\rm el}$ at 565 and 300 K to $(1/\tau_{\rm el\ inter})_b$, then the ratio in Eq. (63) must be ~ 2 and we find for both the case $T_{\rm el}=665$ and 765 K at $T_L=565$ K, $|M|^2_{\rm intra}/|M|^2_{\rm inter}\sim 1$. While this result is probably fortuitously close to 1, since approximations have been made in obtaining Eq. (63), these calculations suggest that $|M|^2_{\rm intra}$ and $|M|^2_{\rm inter}$ are roughly the same.

The energy relaxation rate of Eq. (56) for band (2) is due to transfer of energy between the valence band (2) at temperature $T_{\rm el}$ and conduction band (1) at temperature T_L. This kind of increase in effective relaxation rate with band crossing is consistent with the observations of Schoenlein *et al.*,[35] in their study of the effect of overlapping bands in the GaAs-GaAlAs alloys. The difference is that in their experiments electrons pumped into the conduction band transfer into a subsidiary band which is empty.

In recent high power DECP experiments in Sb,[36] it has been observed that $(1/\tau_{\rm el})$ probably increases with pump-pulse power, although this interpretation of the data is complicated by the observation that $(1/\tau_{\rm ph})$ also appears to increase with power. One contribution to the increase of $(1/\tau_{\rm el})$ with pump power could be an increase in ϵ_{F_2} at high powers due to pumping of electrons out of band (2) (see Fig. 9), leading to more hole states available in band (2) for scattering of cool electrons from band (1), and resulting in a faster relaxation rate.

It is also interesting to consider the result obtained for $(1/\tau_{\rm el\ inter})_b$ in the limiting case of sharply defined Fermi levels in bands (1) and (2), and to compare this with the expression for $(1/\tau_I)$ obtained in Refs. 30 and 31. For this calculation, we will assume that $\hbar\omega_0 \ll kT_L, kT_{\rm el}$. The assumption of sharply defined Fermi surfaces means that ϵ_{F1} and ϵ_{F2} are both large compared to $k_BT_{\rm el}$ and k_BT_L. We also assume that the number of electrons removed from band (2) by the pump pulse is small compared to the number of holes present before the pulse, so that the Fermi level is not shifted appreciably. Both the numerator and denominator in Eq. (56) must be evaluated by expansion about the Fermi energy, as both consist of the difference between nearly equal large terms, and the residual differences come mainly from contributions near the Fermi energy (see Fig. 9). If we assume that $\hbar\omega_0/kT_{\rm el}$ and $\hbar\omega_0/kT_L$ are both small compared to 1, then $\hbar\omega_0$ can be neglected in Eq. (57). Expanding the energy and density of states factors in Eq. (56) about the Fermi energy ϵ_{F2} in the valence band, and using the condition, Eq. (26), that the number of holes in band (2) equals the number of electrons in band (1) leads to the relation

$$N_1 m_1^{\star 3/2}\epsilon_{F_1}^{3/2} = N_2 m_2^{\star 3/2}\epsilon_{F_2}^{3/2}, \tag{64}$$

and Eq. (56) becomes

$$\left(\frac{1}{\tau_{\rm el\ inter}}\right)_b = \frac{1}{2}\left(\frac{2\pi}{\hbar}\right)|M|^2_{\rm inter} V \times N_1 C_1(\epsilon_{F1})^{1/2} \times [1-\tfrac{1}{3}\rho][2n(T_L)+1], \tag{65}$$

where

$$\rho = \left(\frac{N_1}{N_2}\right)^{2/3}\left(\frac{m_1^\star}{m_2^\star}\right) = \left(\frac{\epsilon_{F2}}{\epsilon_{F1}}\right). \tag{66}$$

Equation (65) can be compared with the interband number relaxation rate $1/\tau_I$ (discussed in Sec. IV), when the valence and conduction bands are both at temperature T_L, but the Fermi levels between carriers in the two bands have been displaced by a deformation of the lattice occurring during a lattice vibration (see Fig. 9). This case has been considered by Lopez[31] and Lopez and Koenig[30] in their discussion of the acoustoelectric effect in Bi. They calculate $1/\tau_R$ (equivalent to our $1/\tau_I$) for the case of sharply defined Fermi levels in both conduction and valence bands, but they do not make the simplifying assumption that $\hbar\omega_0$ is much less than k_BT. They obtain an excellent fit to their measurements of $1/\tau_R$ over the entire temperature range from $\sim$4 K to $\sim$100 K. The fit they obtain requires the presence of both acoustic and optical mode contributions, but the optical mode contribution dominates at temperatures of $\sim$100 K and higher. For high temperatures, at which it is appropriate to treat $\hbar\omega_0$ as small compared to k_BT, their result can be written, in our notation, in the form

$$\frac{1}{\tau_I} = \frac{1}{2}\left(\frac{2\pi}{\hbar}\right)|M|^2_{\rm inter} V \times N_1 C_1(\epsilon_{F1})^{1/2} \times [1+\rho^{-1}] \times [2n(T_L)+1]. \tag{67}$$

The ratio of $1/\tau_I$ to $(1/\tau_{\rm el\ inter})_b$ is thus

$$\frac{1/\tau_I}{(1/\tau_{\rm el\ inter})_b} = \frac{[1+\rho^{-1}]}{[1-\frac{1}{3}\rho]}, \tag{68}$$

and Eq. (66) can be used to replace ρ by $(\epsilon_{F2}/\epsilon_{F1})$.

Equation (68) holds for the case of overlapping bands with sharply defined Fermi levels ϵ_{F1} and ϵ_{F2} in both bands, and with $k_BT_{\rm el}$ and k_BT_L greater than $\hbar\omega_0$. It should be noted that Eq. (68) is the result if the heated carriers are in the valence band (2). If heated carriers are instead electrons in band (1), then the labels (1) and (2) in Eq. (67) are reversed. If the relation Eq. (68) holds roughly for Ti_2O_3 after band crossing, and we take $\rho^{3/2}\sim$ 2 to 3 as suggested by Table I in Sec. IV, then we find the ratio in Eq. (68) to be

$$\frac{1/\tau_I}{(1/\tau_{\rm el\ inter})_b} \cong 3.5 \text{ to } 5. \tag{69}$$

If we further assume that $(1/\tau_{\rm el\ inter})_b$ is 2/3 the electron relaxation rate after band crossing then we find $\omega_0\tau_I \sim 4$ to 6. This would imply that the charge oscillating between bands (1) and (2) during an $A_{1g\ell}$ oscillation cycle is very small, and the contribution to Eqs. (23) and (24) is negligible. $\rho^{3/2}$ would have to be as large as 4.68, for $\omega_0\tau_I$ to be $\sim$1.

VI. PHONON RELAXATION

As for the case of spin resonance damping, the relaxation rate for the $A_{1g\ell}$ mode excited by DECP consists of two parts:

$$\frac{1}{\tau_{\rm ph}} = \left(\frac{1}{\tau_{\rm ph}}\right)_1 + \left(\frac{1}{\tau_{\rm ph}}\right)_2, \tag{70}$$

where $\tau_{\rm ph1}$ is analogous to the spin energy relaxation time T_1 and $\tau_{\rm ph2}$ is the analogue of the spin dephasing time T_2. One possible source of $(1/\tau_{\rm ph})_1$ is the inelastic three-phonon process in which the coherent $\vec{Q}=0$ optical phonon of angular frequency ω_0 excited in DECP loses energy by the emission of two acoustic phonons of angular frequency $\omega_0/2$ and of equal and opposite $\vec{Q}$ vectors. For a description of this mechanism, the wave function of the $A_{1g\ell}$ coherent state excited by the pump pulse can be written

$$\psi(q,t) = \sum_\ell c_\ell(t)\psi_\ell(q)\exp[-i(\ell+1/2)\omega_0 t], \tag{71}$$

where ℓ is a harmonic oscillator quantum number for the A_{1g} phonon mode and q is the A_{1g} displacement coordinate. The coefficients $c_\ell(0)$ immediately after the pump pulse are

those of the well-known solution[37] of the problem of the displaced harmonic oscillator wave packet. The coefficients $c_{\ell}(0)$ are given by[37]

$$c_{\ell}(0)=e^{-\lambda^2}\lambda^{\ell}\sqrt{\frac{2^{\ell}}{\ell!}}, \tag{72}$$

where

$$\lambda\equiv\frac{\Delta q_{\rm eq}}{\sqrt{2}\overline{q}} \tag{73}$$

($\Delta q_{\rm eq}$) is the displacement of the equilibrium value of q after the pump pulse, and $\overline{q}$ is the root mean squared value of the displacement in the $A_{1g\ell}$ mode ground state before the arrival of the pump pulse, given by Eq. (37).

The oscillations in amplitude of the reflectivity are produced by the oscillations in the displacement of the center of the oscillator wave packet during DECP. The reflectivity is modified by changes in dielectric behavior produced by band edge motion due to the $A_{1g\ell}$ vibration through the mechanism of the deformation potential. An expression for the decay rate of the amplitude of oscillations of the wave packet due to two-phonon emission, immediately after the arrival of the pump pulse, can be obtained by the use of the equation of motion of the wave packet density matrix in the relaxation approximation. The result obtained is

$$\langle\dot{q}\rangle=-\frac{2\pi}{\hbar}|M|^2\rho\left(\frac{\hbar\omega_0}{2}\right)\left[\left\{n_Q\left(\frac{\omega_0}{2}\right)+1\right\}\left\{n_{-Q}\left(\frac{\omega_0}{2}\right)+1\right\}-\left\{n_Q\left(\frac{\omega_0}{2}\right)\right\}\left\{n_{-Q}\left(\frac{\omega_0}{2}\right)\right\}\right]\times\frac{3}{2}\langle q\rangle. \tag{74}$$

In Eq. (74), $\langle q\rangle$ is the mean amplitude of the displaced wave packet, and $\rho(\hbar\omega_0/2)$ is the density of states in energy of the phonon spectrum at frequency $\omega_0/2$ available for scattering. $|M|^2$ is the matrix element squared for the two phonon decay process. The first term in brackets is a two-phonon emission term for phonons at frequency $\omega_0/2$ and wave vectors $\vec{Q}$ and $-\vec{Q}$. The second term is due to two-phonon absorption, and $n_Q(\omega_0/2)=n_{-Q}(\omega_0/2)$ is the phonon population factor at temperature T_L.

Equation (74) leads to an expression for the three-phonon contribution to $(1/\tau_{\rm ph})_1$ of the form

$$\left(\frac{1}{\tau_{3\rm ph}}\right)_1=\frac{3\pi}{\hbar}|M|^2\rho(\hbar\omega_0/2)[2n(\omega_0/2)+1]. \tag{75}$$

If the change in $\rho(\hbar\omega_0/2)$ and $n(\omega_0/2)$ due to the band crossing is neglected, then all of the temperature dependence of this contribution to $(1/\tau_{\rm ph})_1$ is given by the change in temperature T_L and its effect on $n(\omega_0/2)$. Superposed on the experimental data for $1/\tau_{\rm ph}$ in Fig. 5 we show a dashed line plot of the temperature dependence of Eq. (75), scaled to fit the experimental data at room temperature. We see that the three-phonon contribution to $(1/\tau_{\rm ph})_1$ is capable of explaining about 2/3 of the rise in $(1/\tau_{\rm ph})$ observed between $T_L=300$ K and $T_L=600$ K.

There is another possible source of damping of the coherent phonon excited in DECP in which energy is taken from the coherent $A_{1g\ell},\vec{Q}=0$ optical phonon state by an electron which then scatters with the emission of an incoherent optical phonon of $\vec{Q}\neq 0$ and nearly the same energy. Energy and momentum would be conserved in the electron scattering. Since this process is first order in the incoherent optical phonon, we expect the difference between the emission and reverse absorption process to be independent of the scattered phonon population. On the other hand, the damping rate due to this process should depend on the availability of electron states for scattering, approximately in the same way as $(1/\tau_{\rm el})$ depends on the availability of such states. We therefore expect this two-phonon contribution to $(1/\tau_{\rm ph})_1$ to be of the form

$$\left(\frac{1}{\tau_{2\rm ph}}\right)_1\cong K\left(\frac{1}{\tau_{\rm el}}\right), \tag{76}$$

where K is a constant and therefore to depend on lattice temperature T_L. In Fig. 5 we show a plot of an attempt to fit the data with an expression of the form

$$\left(\frac{1}{\tau_{\rm ph}}\right)_1=K_3\left(\frac{1}{\tau_{3\rm ph}}\right)_1+K\left(\frac{1}{\tau_{\rm el}}\right). \tag{77}$$

Although the fit of the data is better than that shown for $(1/\tau_{3\rm ph})$, alone, the result is unconvincing, given the scatter of the data points. In any case, the proportions in which two- and three-phonon energy loss and dephasing contribute to the effective phonon relaxation rate is not clear.

It should be noted that a contribution of the form of Eq. (76) could contribute to an increase in $(1/\tau_{\rm ph})$ observed in high power DECP experiments performed in Sb.[36]

VII. DISCUSSION

Equation (68) relating $(1/\tau_I)$ and $(1/\tau_{\rm el\ inter})_b$, although only a rough approximation at 300 K, should apply to other materials such as Bi and Sb, both of which have been studied in optical pump-probe experiments.[2] $(1/\tau_{\rm el})$ for Bi and Sb at room temperature were found to be $\sim 0.1\times 10^{12}\ {\rm s}^{-1}$ and $0.6\times 10^{12}\ {\rm s}^{-1}$, respectively, although the former number was not determined very accurately because the decay was slow and the signal relatively weak.

$(1/\tau_I)$ has only been measured for Bi up to $T\sim 50$ K.[31] Extrapolating Lopez's excellent theoretical fit of his data to $T=300$ K yields $(1/\tau_I)\cong 2.6\times 10^{12}\ {\rm s}^{-1}$ for Bi. From tabulated values of $(\epsilon_{\rm Fh}/\epsilon_{\rm Fe})$ for Bi (Ref. 38) we find $\rho\cong 0.42$ or $\rho\cong 2.4$, depending, respectively, on whether valence band carriers or conduction band carriers are heated by the pump pulse [see discussion after Eq. (68)]. These values of ρ, inserted into Eq. (68) and combined with the extrapolated values of $(1/\tau_I)$, lead to predicted rates $(1/\tau_{\rm el\ inter})_b$ of $0.66\times 10^{12}\ {\rm s}^{-1}$ or $0.34\times 10^{12}\ {\rm s}^{-1}$, depending respectively on whether valence band or conduction band carriers are heated. These numbers are to be compared with the measured value of $(1/\tau_{\rm el})\cong 0.1\times 10^{12}\ {\rm s}^{-1}$. Considering the uncertainty in the experimental value as well as the calculated result, the agreement is reasonable, and suggests that conduction band heating might be dominant in Bi.

The measured value of $0.6\times 10^{12}\ {\rm s}^{-1}$ for the value of $(1/\tau_{\rm el})$ in Sb is much more accurate than the value obtained for Bi. If we take $\sim 2/3$ of this value (as for the case of

Ti_2O_3) as a rough estimate for $(1/\tau_{\text{el inter}})_b$, then we can use tabulated band structure parameters for Sb to estimate ρ, and thus use Eq. (68) to predict $(1/\tau_I)$. We find $\rho=0.65$ or $\rho=1.53$, respectively, for valence band or conduction band carrier heating. Equation (68) then yields $(1/\tau_I)=1.3\times10^{12}$ s^{-1} or 2.8×10^{12} s^{-1}, depending, respectively, on whether valence band carriers or conduction band carriers were heated in the optical pump-probe experiments on Sb. These predicted values of $(1/\tau_I)$ for Sb seem to be in a reasonable range, compared with the extrapolated experimental value for Bi of $(1/\tau_I)\cong2.6\times10^{12}$ s^{-1} at $T=300$ K.

There is an interesting analogy between the A_1 ''displacement field'' in a solid, which lowers the symmetry of a crystal, and the Higgs field which is associated with the symmetry breaking of the vacuum. This analogy is particularly striking in the case of the Bi structure, where the A_{1g} displacement lowers the symmetry from cubic to trigonal. In the related $Ge_{1-x}Pb_xTe$ structure, the phase transition from trigonal back to cubic can be followed by increasing the temperature. In both the crystal and vacuum cases, the final equilibrium ''displacement'' is determined by the minimization of the free energy at ambient temperature. In a DECP experiment in a crystal, electronic excitation changes the quasiequilibrium A_1 displacement, tending to restore the higher symmetry state. If the excitation occurs in a time short compared to an A_1 vibration period, the lattice is set into A_1 vibration about the new equilibrium displacement. Similarly, excitation of the vacuum by the creation of a high energy plasma of particles should shift the quasiequilibrium Higgs field displacement toward the vacuum of unbroken symmetry. If enough energy has been added to the vacuum in a short enough time, it should, in principle, be possible to excite coherent ''phonons'' associated with the Higgs field. A heating of the vacuum back to a free quark-gluon plasma state has been suggested as a possibility in high energy heavy ion-ion collisions.[39] However, the initial rise in excitation in such collisions would have to be extraordinarily rapid to produce a DECP-like excitation. If, for example, the mass of the boson associated with the Higgs field were greater than 41 GeV,[40] the excitation of the vacuum would have to take place in a time $t\lesssim10^{-25}$ s. For comparison, the time for a relativistic particle to travel 10^{-13} cm is $t\sim3\times10^{-24}$ s.

ACKNOWLEDGMENTS

We are grateful to Dr. Alan Strauss of Lincoln Laboratory for his continuing interest in this work. We thank Dr. Alan Strauss and Robert Fahey for providing the Ti_2O_3 samples and for advice in the handling of these materials. Discussions of the Higgs field with Professors Francis Low and Patrick Lee are gratefully acknowledged. We acknowledge NSF Grant No. DMR-95-10093 for support of this work.

[1] T. K. Cheng, J. Vidal, H. J. Zeiger, G. Dresselhaus, M. S. Dresselhaus, and E. P. Ippen, Appl. Phys. Lett. **59**, 1923 (1991).
[2] H. J. Zeiger, J. Vidal, T. K. Cheng, E. P. Ippen, G. Dresselhaus, and M. S. Dresselhaus, Phys. Rev. B **45**, 768 (1991).
[3] T. K. Cheng, S. D. Brorson, A. S. Kazeroonian, J. S. Moodera, G. Dresselhaus, M. S. Dresselhaus, and E. P. Ippen, Appl. Phys. Lett. **57**, 1004 (1990).
[4] G. C. Cho, W. Kütt, and H. Kurz, Phys. Rev. Lett. **65**, 764 (1990).
[5] J. M. Chwalek, C. Uher, J. F. Whitaker, G. A. Mourou, and J. A. Agostinelli, Appl. Phys. Lett. **58**, 980 (1991).
[6] T. K. Cheng, S. D. Brorson, A. Kazeroonian, J. S. Moodera, G. Dresselhaus, M. S. Dresselhaus, and E. P. Ippen, in *Extended Abstracts of the Symposium on Electronic, Optical and Device Properties of Layered Structures*, edited by J. Hayes, M. S. Hybertsen, and E. R. Weber (Materials Research Society, Pittsburgh, PA, 1990).
[7] H. Kurz, QELS Digest **11**, 58 (1991).
[8] T. K. Cheng, L. Acioli, E. P. Ippen, J. Vidal, H. J. Zeiger, and M. S. Dresselhaus, Appl. Phys. Lett. **62**, 1901 (1993).
[9] K. Seibert, H. Hensel, T. Albrecht, J. Gerits, K. Allenkbverdiev, and H. Kurz, Proc. 20th Int. Conf. Phys. Semicond. **3**, 1981 (1990).
[10] C. N. R. Rao, R. E. Loehman, and J. M. Honig, Phys. Lett. **27A**, 271 (1968).
[11] C. E. Rice and W. R. Robinson, Acta Crystallogr. B **33**, 1342 (1977).
[12] H. L. Barros, G. V. Chandrasekhar, T. C. Chi, J. M. Honig, and R. J. Sladek, Phys. Rev. B **7**, 5147 (1973).
[13] S. H. Shin, R. L. Aggarwal, B. Lax, and J. M. Honig, Phys. Rev. B **9**, 583 (1974).
[14] G. Luckovsky, J. W. Allen, and P. Allen, Inst. Phys. Conf. Ser. **43**, 465 (1979).
[15] J. Yahia and H. P. R. Frederikse, Phys. Rev. **123**, 1257 (1961).
[16] J. M. Honig and T. B. Reed, Phys. Rev. **174**, 174 (1968).
[17] S. H. Shin, G. V. Chandrashekhar, R. E. Loehman, and J. M. Honig, Phys. Rev. B **8**, 1364 (1973).
[18] J. B. Goodenough, in *Proceedings of the 10th International Conference Physics of Semiconductors*, edited by S. P. Keller, J. C. Hensel, and F. Stern (U.S. Atomic Energy Commission, Oak Ridge, TN, 1970), p. 304.
[19] J. Ashkenazi and M. Weger, J. Phys. (Paris) Colloq. **37**, C4-189 (1976).
[20] H. J. Zeiger, T. A. Kaplan, and P. M. Raccah, Phys. Rev. Lett. **26**, 1328 (1971).
[21] H. J. Zeiger, Phys. Rev. B **11**, 5132 (1974).
[22] Landolt and Börnstein, in *Numerical Data and Functional Relationships in Science and Technology* (Springer–Verlag, Berlin, 1983), Vol. III, p. 151.
[23] R. L. Fork, B. I. Greene, and C. V. Shank, Appl. Phys. Lett. **38**, 671 (1981).
[24] E. P. Ippen and C. V. Shank, in *Ultrashort Light Pulses*, edited by S. L. Shapiro (Springer-Verlag, Berlin, 1984), Chap. 3, p. 83.
[25] Jordina Vidal, Ph.D. thesis, Massachusetts Institute of Technology, 1994.
[26] X. Gonze, J.-P. Michenaud, and J.-P. Vigneron, Phys. Rev. B **41**, 11 827 (1990).
[27] S. S. M. Lu, F. H. Pollack, and P. M. Raccah, Phys. Rev. B **17** (1978).
[28] R. H. M. Groeneveld, R. Sprik, and A. Lagendijk, Phys. Rev. B **45**, 5079 (1992).

[29] F. Cerdeira and M. Cardona, Phys. Rev. B **9**, 1440 (1972).
[30] A. A. Lopez and S. H. Koenig, Solid State Commun. **4**, 513 (1966).
[31] A. A. Lopez, Phys. Rev. **175**, 823 (1968).
[32] J. McDougall and E. C. Stoner, Philos. Trans. R. Soc. A **237**, 67 (1938).
[33] P. B. Allen, Phys. Rev. Lett. **59**, 1460 (1987).
[34] J. M. Ziman, *Electrons and Phonons* (Clarendon Press, Oxford, 1960).
[35] R. W. Schoenlein, W. Z. Lin, J. G. Fujimoto, and G. L. Eesley, Phys. Rev. Lett. **58**, 1680 (1987).
[36] Tak Keung Cheng, Ph.D. thesis, Massachusetts Institute of Technology, 1994.
[37] D. Bohm, *Quantum Theory* (Clarendon Press, Oxford, 1951), p. 306.
[38] Landolt and Börnstein, in *Numerical Data and Functional Relationships in Science and Technology* (Ref. 22), Vol. III/13c, p. 65. Berlin, Heidelberg, NY, 1983).
[39] S. Das Gupta and G. D. Westfall, Phys. Today **46**, 34 (1993).
[40] R. Hempfling, Phys. Lett. B **296**, 121 (1992).